

January 2015

Preparation And Characterization Of Self-Assembled Monolayers And Mesoscale Protein Patterning

Panae Noomuna
Eastern Kentucky University

Follow this and additional works at: <https://encompass.eku.edu/etd>

 Part of the [Chemistry Commons](#)

Recommended Citation

Noomuna, Panae, "Preparation And Characterization Of Self-Assembled Monolayers And Mesoscale Protein Patterning" (2015).
Online Theses and Dissertations. 300.
<https://encompass.eku.edu/etd/300>


This Open Access Thesis is brought to you for free and open access by the Student Scholarship at Encompass. It has been accepted for inclusion in Online Theses and Dissertations by an authorized administrator of Encompass. For more information, please contact Linda.Sizemore@eku.edu.

PREPARATION AND CHARACTERIZATION OF SELF-ASSEMBLED
MONOLAYERS AND MESOSCALE PROTEIN PATTERNING

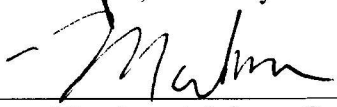
By

Panae Noomuna

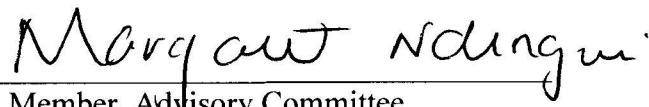
Thesis Approved:




Chair, Advisory Committee



Member, Advisory Committee



Member, Advisory Committee



Dean, Graduate School

STATEMENT OF PERMISSION TO USE

In presenting this thesis in partial fulfillment of the requirements for a Master's degree at Eastern Kentucky University, I agree that the Library shall make it available to borrowers under rules of the Library. Brief quotations from this thesis are allowable without special permission, provided that accurate acknowledgment of the source is made.

Permission for extensive quotation from or reproduction of this thesis may be granted by my major professor, or in his absence, by the Head of Interlibrary Services when, in the opinion of either, the proposed use of the material is for scholarly purposes. Any copying or use of the material in this thesis for financial gain shall not be allowed without my written permission.

Signature  _____

Date 04/13/2015

PREPARATION AND CHARACTERIZATION OF SELF-ASSEMBLED
MONOLAYERS AND MESOSCALE PROTEIN PATTERNING

By

Panae Noomuna

Bachelor of Education (Science)

University of Nairobi

Nairobi, Kenya

2010

Submitted to the Faculty of the Graduate School of

Eastern Kentucky University

in partial fulfillment of the requirements

For the degree of

MASTER OF SCIENCE

May, 2015

Copyright© Panae Noomuna, 2015

All rights reserved.

DEDICATION

This thesis is dedicated to my parents; Resiato Ene Kirrinkai Noomuna and Kirrinkai Ole Morijoi, and my brother Saruni Noomuna for the opportunities and experiences they have offered me that have made me who I am today. I will be forever indebted to you for your selfless contributions in helping me seek my own destiny.

ACKNOWLEDGEMENTS

First I am grateful to God whom without his sufficient grace, I wouldn't have been able to have this done, for good health and wellbeing which were necessary to complete this paper.

Secondly, this thesis would not have been possible without the inspiration and support of a number of wonderful individuals.

I owe my deepest express and sincere gratitude to my adviser, Dr. Pei Gao for her patience and invaluable guidance and encouragement extended to me. Your continuous optimism, enthusiasm and faith in my work has kept me in line. You have been a tremendous mentor to me. Your support has been priceless. Thank you.

To my advisory committee members; Dr, Margaret Ndinguri and Dr. Martin Brock, it has been amazing having you in the committee. Thank you for sharing your expertise and wisdom with me. I am grateful to you.

To Andrew Schlereth for his laboratory contributions which immensely contributed to my thesis completion. Thank you.

I am grateful to Eastern Kentucky Chemistry Department, Kentucky Biomedical Research Infrastructure Network (KBRIN) and Kentucky's National Science Foundation Experimental Program to Stimulate Competitive Research (KY EPSCoR) for their financial support.

A special thanks to my parents Resiato Ene Kirrinkai Noomuna and Kirrinkai Ole Morijoi. Words cannot express how thankful I am for the sacrifices you have made on my behalf. Education is the ultimate inheritance a parent can give to a child. You have so selflessly and lovingly walked this journey with me. You are wonderful and am grateful to both of you.

To my brothers and sisters; sometimes half what we need to get to our destinations is siblings' support, your love and support is an incentive I needed to get towards my goals. You have been an inspiration. Thank you.

And to all who directly or indirectly contributed to the completion of this journey, I may not be able to mention you name by name but I wish to extend special regards to you. Your calls, personal messages and your time to time checking on me has kept me sane during this period of my life. You provided the so much needed break from an otherwise hectic rush. I am so grateful to you. May God reward you according to his heavenly riches.

ABSTRACT

Bottom-up approach was used to develop self-assembled monolayers of octadecyltrichlorosilane (OTS) and undecenyltrichlorosilane(UTS) on Si(100) wafer. Undecenyltrichlorosilane monolayer was oxidized at the vinyl terminal to generate a carboxylic acid group. Lysozyme protein was immobilized on the polar carboxylic acid group. The developed protein patterns were investigated using fluorescence microscopy. Lysozyme has an isoelectronic point of 11.35. At a pH below this value the protein is positively charged making it a good candidate for electrostatic adsorption on the negatively charge $-\text{COO}^-$ group. Fluorescence images confirm formation of lysozyme across the silicon wafer. The patterned Si(100) wafer can be used as a biosensor against lysozyme antibodies.

Another approach to develop varied surface properties was used to grow OTS on oxidized UTS_x via chemical phase deposition (CVD). In this case we used polystyrene and silicon nanospheres as masking agents on the already developed and oxidized UTS. Fluorescence images revealed that OTS layers were formed on the interstitial spaces of the nanosphere masks. Varied protein can be immobilized on this surface due to different terminal groups on the surface.

KEYWORDS: Self-Assembled Monolayers, Mesoscale protein patterns, Nanosphere lithography, Lysozyme, Fluorescence microscopy

TABLE OF CONTENTS

| | |
|--|-----|
| CHAPTER 1 BACKGROUND AND INTRODUCTION | xii |
| 1.1 Introduction | 1 |
| 1.2 Lithographic Techniques..... | 5 |
| 1.1.1 Photolithography | 5 |
| 1.1.2 Electron beam lithography..... | 8 |
| 1.1.3 Nanosphere Lithography | 9 |
| 1.3 Self-Assembled Monolayers (SAMs) | 13 |
| 1.2.1 Introduction | 13 |
| 1.2.2 Types of Self-Assembled Monolayers | 14 |
| 1.4 Objectives of this Thesis | 18 |
| 1.5 Organization of this Thesis | 19 |
| CHAPTER 2 INSTRUMENTATION | 20 |
| 2.1 Fluorescence Microscopy..... | 20 |
| 2.1.1 Introduction | 20 |
| 2.1.2 Principles of Fluorescence..... | 21 |
| 2.1.3 Fluorescence Microscope | 24 |
| 2.1.4 Conclusion | 26 |
| 2.2 Fourier Transform Infrared Spectroscopy (FTIR) | 27 |
| 2.2.1 Introduction | 27 |

| | |
|---|-----------|
| 2.2.2 The Fourier Transform Infrared (FT-IR) Spectrometer | 30 |
| 2.2.3 Interpretation of infrared spectrum..... | 31 |
| 2.2.4 Conclusion | 32 |
| 2.3 Atomic Force Microscopy (AFM) | 33 |
| 2.3.1 Introduction | 33 |
| 2.3.2 Basic working principle of atomic force microscope..... | 34 |
| 2.3.3 Conclusion | 36 |
| CHAPTER 3 PREPARATION AND CHARACTERIZATION OF SELF ASSEMBLED MONOLAYERS..... | 37 |
| 3.1 Introduction | 37 |
| 3.2 Experimental: To prepare and characterize self-assembled monolayers | 39 |
| 3.2.1 Materials | 39 |
| 3.2.2 Procedure I: Preparation of SAMs..... | 40 |
| 3.2.3 Characterization of octadecyltrichlorosilane SAMs..... | 42 |
| 3.2.4 Procedure II: Preparation and Oxidation of UTS SAMs..... | 45 |
| 3.2.5 Characterization of UTSox..... | 47 |
| 3.2.6 Conclusion | 49 |
| CHAPTER 4 FABRICATION AND CHARACTERIZATION OF PROTEIN PATTERNS BASED ON NANOSPHERE LITHOGRAPHY | 50 |
| 4.1 Introduction | 50 |

| | |
|--|----|
| 4.2 Experimental I: Nanofabrication of protein patterns on UTSox | 53 |
| 4.2.1 Materials | 53 |
| 4.2.2 Procedure I: Immobilization of Lysozyme | 54 |
| 4.2.3 Characterization of protein patterns. | 56 |
| 4.3 Experimental II: Preparation of multilayers of self-assembled monolayers. | 58 |
| 4.3.1 Materials | 58 |
| 4.3.2 Procedure II: Preparation of OTS Layer on UTSox | 58 |
| 4.3.3 Characterization of OTS-UTSox multi-layers..... | 61 |
| 4.4 Conclusion..... | 65 |
| CHAPTER 5 CONCLUSIONS AND FUTURE DIRECTIONS | 66 |
| 5.1 Conclusions | 66 |
| 5.2 Challenges of the Research | 67 |
| 5.3 Future Directions..... | 69 |
| 5.4 Concluding Remarks | 70 |

LIST OF TABLES

| | |
|---|---|
| Table 1.1. Comparison of Apollo 11 Guidance Computer (1969) and Samsung S5 Smartphone (2014). Source: Samsung website, Online. (Accessed 3/5/2015). Source: Finder's Free Website, Online: (Accessed 3/5/2015). Source: NASA website, Online: (Accessed 3/5/2015)..... | 3 |
|---|---|

LIST OF FIGURES

| | |
|--|----|
| Figure 1.1. Illustration of general working principle of photolithography. | 6 |
| Figure 1.2. Schematic illustration of electron beam lithography. | 8 |
| Figure 1.3. Illustration of Nanosphere lithography process (Top view)..... | 10 |
| Figure 1.4. Illustration of interstitial distances and in-plane diameters of periodic particle arrays. Source: Department of Materials Science and Engineering, Northwestern University. (Accessed 03/10/2015)..... | 12 |
| Figure 1.5. Basic features of self-assembled monolayers..... | 13 |
| Figure 1.6. Schematic representation of fatty acid monolayers on AgO and Al ₂ O ₃ ; Reprinted with permission from ref. ²⁰ Copyright (1996) American Chemical Society. .. | 16 |
| Figure 1.7. Schematic representation of OTS monolayer on Silicon wafer. | 17 |
| Figure 2.1. Jablonski diagram showing absorption and emission of light by a fluorophore. | 22 |
| Figure 2.2. Working principle of fluorescence microscope..... | 25 |
| Figure 2.3. Electromagnetic spectrum. Source: Natural science Inc1 with None at Western Governors University. Online: (Accessed 1/28/2015)..... | 27 |
| Figure 2.4. Working principle of single-beam FT-IR spectrometer. | 30 |
| Figure 2.5. Illustration of working principle of atomic force microscope. | 35 |
| Figure 3.1. Schematic representation of growth of SAMs in solution..... | 38 |
| Figure 3.2. Structure of self-assembled monolayers used in this research. | 39 |
| Figure 3.3. Illustration of formation of octadecyltrichlorosilane on Silicon surface. | 42 |
| Figure 3.4. AFM Topography and Phase images of OTS in 50×50 μm ² area. | 44 |

| | |
|--|----|
| Figure 3.5. FT-IR spectra of OTS monolayer on silicon surface..... | 44 |
| Figure 3.6. Illustration of surface oxidation of UTS monolayer..... | 47 |
| Figure 3.7. Brewster angle IR spectra of UTS (red) and UTSox (blue). | 47 |
| Figure 3.8. Scheme for conversion of vinyl group to carboxylic group | 48 |
| Figure 3.9. Illustration of staining UTSox with PDAM. | 49 |
| Figure 4.1. 3-D structure of lysozyme. ⁵⁶ | 53 |
| Figure 4.2. Structure of fluorescein isothiocyanate (FITC). | 54 |
| Figure 4.3. Illustration of coating of UTSox with polystyrene nanospheres | 55 |
| Figure 4.4. Illustration of fabrication of lysozyme patterns on UTSox. | 56 |
| Figure 4.5. Fluorescence image of FITC-tagged lysozyme. Part A represents images taken against white light and B is taken against fluorescent light..... | 57 |
| Figure 4.6. Schematic representation for preparation of multi-layers of SAMs..... | 59 |
| Figure 4.7. Polystyrene nanospheres on UTSox..... | 61 |
| Figure 4.8. Image of silicon nanospheres on UTSox surface. | 62 |
| Figure 4.9. Fluorescence images of polystyrene patterned OTS-UTSox. The green dots indicates parts of the sample which was not occupied by OTS. The center part of the image has been magnified. | 63 |
| Figure 4.10. Fluorescence Image of silicon patterned UTSox sample. A circular zoomed inset is at the center of the image (enlarged green signals). | 64 |
| Figure 5.1. Illustration of point and line defects in nanospheres patterns. | 68 |

CHAPTER 1

BACKGROUND AND INTRODUCTION

1.1 Introduction

The growing interest in nanostructures and nanoparticles has become ubiquitous across the scientific fields. The trends in technology speak volumes about the driving force; the need to miniaturize materials to nano-scale or sub-micron levels. Recent technological advances have witnessed ever shrinking sizes, decreased costs, lesser processing time and larger storage spaces of devices such as computers, phones, cameras, etc.¹⁻³ This paradigm shift in technology, can be elucidated by the following two reflections of history of technology: technological trends as at 1989 as reported by Bradford et al, and a further tabular comparison of the 1969 then prized computing power of Apollo 11 guidance computers and the 2014-launched Samsung Galaxy S5, thereafter. In 1989, 9600-baud modems retails at \$ 800 each while the available laptops weighing 15 lbs. on average, cost \$ 3000 each. The laptops were not only bulky and expensive, but also scarce. Mobile phones at the same time were not any better; they were cumbersome and each can be purchased at an estimated amount of \$ 1500.⁴

For comparative purposes take a look at **Table 1.1** which outlines the differences between Apollo 11 computers and Samsung Galaxy S5 smartphone revealing some importance of nanotechnology. Apollo 11 guidance computers are those computers that

were used to successfully launch the first rocket to the moon. It is so amazing that the computing power of the current phones is more than that of the 1969 computers; many thanks to the artistic reasoning of Richard Feynman presented in his 1959 famous lecture entitled: 'There's Plenty of Room at the Bottom'. Richard P. Feynman explored the possibility of downsizing materials to atomic scale, pinning the benefits of miniaturized materials on vast data storage spaces, microelectronics, biosensors, solar cells and optical devices among others.⁵⁻⁶ However it was not until the invention of the scanning tunneling microscope and atomic force microscope that Feynman's pioneering work got empirically validated.

Table 1.1. Comparison of Apollo 11 Guidance Computer (1969) and Samsung S5 Smartphone (2014). Source: Samsung website, Online. (Accessed 3/5/2015). Source: Finder’s Free Website, Online: (Accessed 3/5/2015). Source: NASA website, Online: (Accessed 3/5/2015).

| Specifics | Apollo 11 Guidance Computer | Samsung S5 Smartphone |
|------------------------------|--|--|
| Dimensions (Inches) | 24 × 12.5 × 6 | 5.59 × 2.85 × 0.32 |
| Weight (lbs) | 70.1 | 0.32 |
| Processor Speed (MHz) | 1 | 2 500 |
| Memory | 4 kB | 16/32 GB in-built, 2 GB RAM |
| Display | 7-segment numeric | 5.1 In, 1080 x 1920 pixels, multi-touch |
| Power consumption (Watts) | 55 | 0.5 – 6.2 |
| Price (US Dollars) | 150 000 | 500 |

The table reveals that nanotechnology would save us money and power consumption, while at the same time ameliorates the production of efficient and effective devices. In other words, minimizing the size of materials (components of devices) and simultaneously taking advantage of their pristine properties at atomic level dramatically reduce power consumption, space (physical), and raises their sensitivity. With a world

facing an impending doom as a result of global warming, devices/machines that save on power consumption are greatly welcomed.

Properties of materials (such as magnetic, catalytic, thermodynamic, and electrical among others) at fine scale are significantly different from those of the bulk matter¹⁻³. An understanding of the evolution of these size-dependent properties, is the starting point towards the realization of technological advancement stated in the preceding text. Two general approaches for producing micro- and nano-sized and/or nanostructured materials are top-down and bottom-up methods.^{2,6}

Top-down approach (very popular in electronics) involves scaling down the bulk matter⁶ to atomic clusters and/or nanostructures/nanoparticles regimes²⁻³ using either precision engineering or lithographic strategies.⁶This is analogous to carving out a statue from wood or stone. As bottom-up strategy, the modus operandi of top-down approach is beyond the scope of this thesis.

Bottom-up method (prominent in nanosphere lithography) employs chemical and/or physical reaction/interaction (as in formation of self-assemblies) of atoms, molecules or nanoparticles to generate compact 2-D or 3-D structures. It is analogous to building a storied building. This method is capable of producing nano-scale features and it is mainly used in the fabrication of self-assembled monolayers that are in turn used as templates for the creation of nanostructures.⁶Unlike top-down there is less material wastage on this approach.

This chapter reviews the general working principle of common lithographic techniques as well as some types of self-assembled monolayers.

1.2 Lithographic Techniques

Lithographic tools fall under two main categories, viz; parallel writing (replication) and sequential writing (patterning). Parallel writing uses masks to generate reproducible patterns on the resist while patterning cast features point by point on the resist.⁶ Various standard fine scale lithographic techniques for fabrication of nanostructures based on bottom-up or top-down methods discussed in the preceding section include, but not limited to the following: photolithography, electron beam lithography and nanosphere lithography. A brief account of each of these techniques is given in the following sub-sections.^{1-3,6.}

1.1.1 Photolithography

As the name suggest, photolithography (the most commonly used process) uses light of a given wavelength to create a pattern on a photoresist (light sensitive material that can polymerize/depolymerize upon exposure to UV light). **Figure 1.1** below details a step by step protocol for fabricating patterns using photolithography.

The starting point of photolithography is cleaning of the wafer to remove any contaminants. Typical wafer's contaminants include dust, bacterial matter, grease and other organic substances. Dust can be minimized if experiments are run in dust free environment and clean room practice. Bacteria, organic matter and other environmental hazards can be cleaned off by rinsing wafers with deionized water, and heating it in a piranha solution (detailed explanation of cleaning a wafer by piranha solution is available in **CHAPTER 3**).⁷

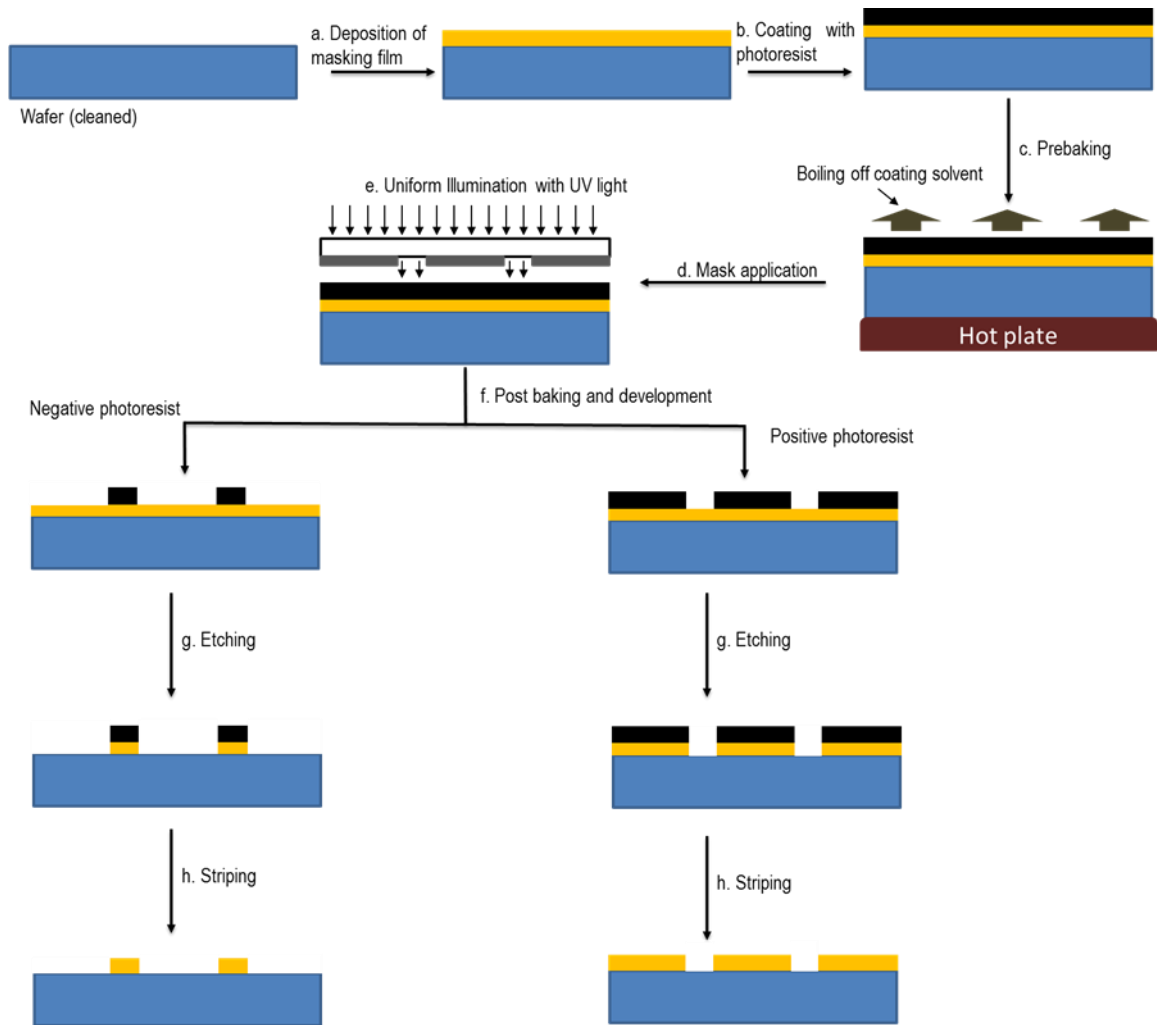


Figure 1.1. Illustration of general working principle of photolithography.

In step (a) (**Figure 1.1**), a uniform thin film layer (masking film); from which patterns would be transferred to the wafer, is applied on to the wafer. Silicon dioxide and silicon nitride are the common masking films used for silicon wafers.^{7,8} In step (b) a photoresist is spin-coated onto the masking film and afterwards evaporating the coating solvent (step c) by prebaking the substrate on a hot plate. Next, a photo-mask (d) is placed above the photoresist. Exposing the photoresist to light (step e) of a given wavelength creates patterns

(the patterns depend on the features of photo-mask used) on the photoresist. Chemical development (step f) remove resists while post-baking (optional process) drives off any remaining coating solvent or developer solution.⁸ For a positive photoresist the chemical structure of areas exposed to radiation changes, making it highly soluble in developer solution and would then be washed away. In the case of a negative photoresist the irradiated areas polymerize and become insoluble in developer solution. The developer solution would wash away unexposed areas of photoresist leaving behind the irradiated regions.

Etching (removal of unwanted material) is done on the patterned photoresist to transfer the patterns to the wafer. Parts exposed to light are removed through chemical (dissolving photoresist in appropriate solvent) or mechanical (stripping) means in the case of a positive photoresist. For a negative photoresist the parts of the resist exposed to light harden and as such would not be removed. Parts not affected by the light are etched away instead.⁹ Common solvents for etching away photoresists include acetone, trichloroethylene for positive photoresist, and methylketone and methyl isobutyl ketone for negative photoresists.⁷After etching, any remaining resist is striped off.

Though the most commonly used form of lithography, conventional optical lithography's resolution is limited by the wavelength of light used. Lithographic resolution (also known as critical dimension; the smallest feature that can be produced on a surface) is related to the wavelength of light used according to the following equation.

$$\text{Resolution} = k_1 \left(\frac{\lambda}{NA} \right) \dots\dots\dots 1.1$$

where k_1 is a constant that dependent on the process being used(values of k_1 range from 0.5 to 0.8), λ is the average wavelength of illuminating light and NA is the numerical

aperture whose values range from 0.5-0.6. Light used can only create features equal or more than the size of its wavelength in size.¹⁰ For instance if the process constant and numerical aperture are 0.5 both, the resolution of the pattern that can be generated by the process is equal to the wavelength of the light used. Resolution limit is one of the disadvantages of photolithography and would therefore not be a good choice lithographic technique for obtaining sub-100 nm features.

1.1.2 Electron beam lithography

Electron beam lithography uses a beam of electrons to directly pattern surfaces of wafers. It is characterized by very high resolution (capable of creating sub-10 nm features) and versatile pattern fabrication.¹¹ **Figure 1.2** illustrates the general procedure of the process.

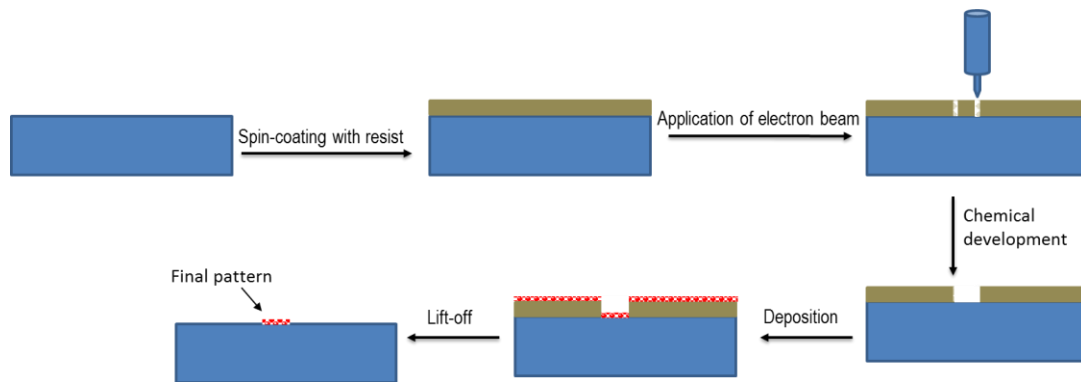


Figure 1.2. Schematic illustration of electron beam lithography.

As can be deduced from the above diagram, an electron sensitive (such as poly-(methyl methacrylate)) resist is uniformly applied onto the substrate. A stream of electrons is then directed on to the resist in a dot to dot manner resulting in a desired pattern. Just as in the case of photolithography the beam of electrons change the chemical structure of the resist making it more soluble in the development solution. The next step is deposition of the sample material such as metal and subsequently lifting-off the resist leaving the material deposited on the part of the substrate that was exposed to the electron beam.¹¹⁻¹²

Electron beam lithography can fabricate patterns as small as 5 nm which makes it preferred over optical lithography for generation of high resolution features but it is very expensive. Because of the high costs associated with electron beam lithography it is not widely used in fabrication of nanostructures.¹²

1.1.3 Nanosphere Lithography

Nanosphere lithography was originally known as natural or colloidal lithography. The term ‘natural’ was first used by Fischer and Zingsheim in 1981 to describe the property of polystyrene latex nanospheres. While investigating replication of submicroscopic features using visible light, they observed that polystyrene latex nanospheres organized themselves (to form a uniform single layer) on a glass substrate.^{3,6,14} In 1982, Deckman and Dunsmuir utilized the idea of Fischer and Zingsheim by using polystyrene nanospheres as large area lithographic masks or deposit materials⁶ to fabricate micro-features of colloidal particles.¹³ They ultimately branded the process as natural/colloidal lithography.^{6,13} Duyne and Hulteen were able to apply the same concept of natural lithography in creation of double layer polymer colloidal masks for studying optical

properties of silver nanoparticles on mica. They described their process as nanosphere lithography, marking the introduction of the term to the nanotechnology field.^{1,6}

A diagrammatic representation of nanosphere lithography process is shown in

Figure 1.3. Illustration of Nanosphere lithography process (Top view)

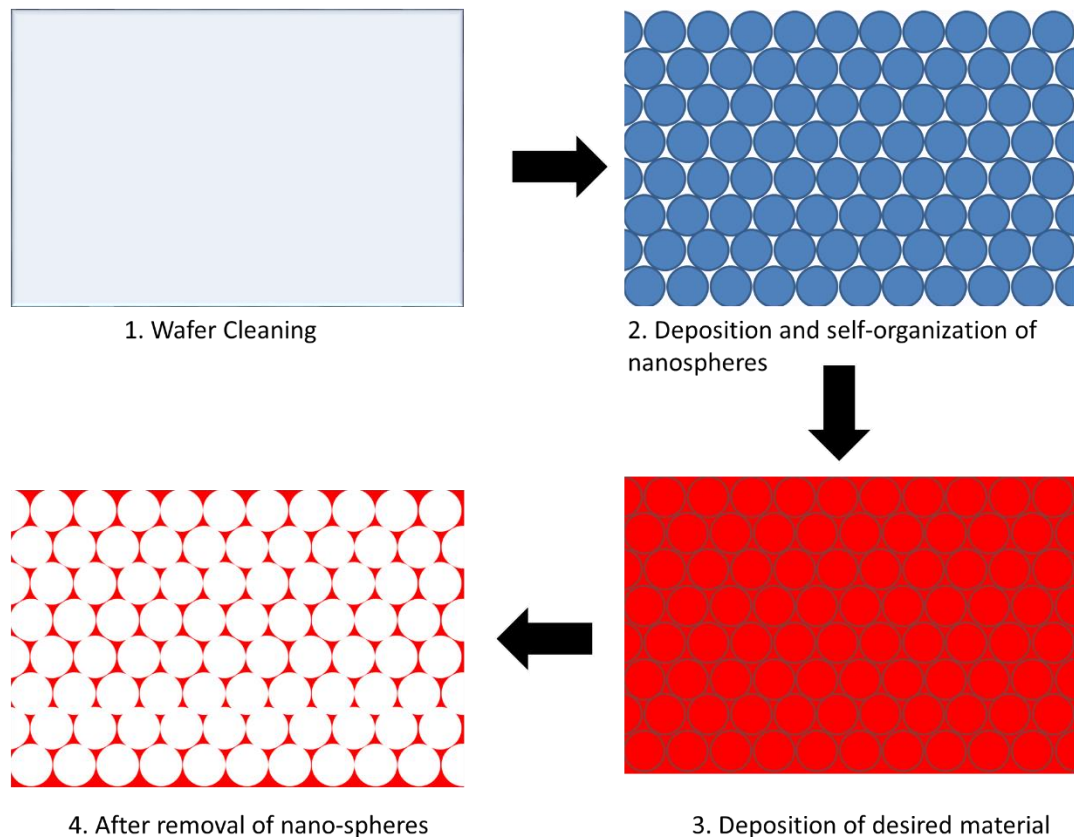


Figure 1.3. Illustration of Nanosphere lithography process (Top view)

Upon deposition on a cleaned substrate, the nanospheres spread themselves uniformly on the surface of the substrate. The material of interest would then be deposited on top of the spheres where it gets adsorbed on the substrate within the interstitial spaces

of the spheres. The nanospheres are removed from the substrate through mechanical (for example stripping)¹ or chemical (sonication in appropriate solvent)⁶ means. This step; commonly known as lift-off, leaves a finger print of the interstitial spaces of the spheres on the substrate occupied by the material deposited. A closer look at the pattern after lift-off on the diagram below, shows triangular-like features that mirror the spaces not covered by the nanospheres while the parts originally covered by spheres appear spherical (in step 4).

The size of the nanospheres used determine the interparticle spacing (see equations below) and illustration of in-plane particle diameter in **Figure 1.4**.

$$d_{ip, SL} = \left(\frac{D}{\sqrt{3}}\right) = 0.577D \dots\dots\dots 1.2$$

$$a_{SL} = \frac{3}{2} \left[\sqrt{3} - 1 - \frac{1}{\sqrt{3}} \right] D = 0.233 D \dots\dots\dots 1.3$$

where $d_{ip, SL}$, is the inter-particle spacing for a monolayer (single layer) of periodic particle arrays and D is the diameter of the nanospheres. The in-plane particle diameter (a) of a single layer (SL) of periodic particle arrays, (see **Figure 1.4**) could also be estimated from the size of the sphere as shown by equation 1.3. In-plane diameter is defined as the distance of a perpendicular bisect of an equilateral triangle that fits the triangular space formed by three adjacent nanospheres.^{1,15} Though not set by the size of the spheres, the out-of-plane height of particle height is approximately equal to the diameter of the film of the material deposited.¹

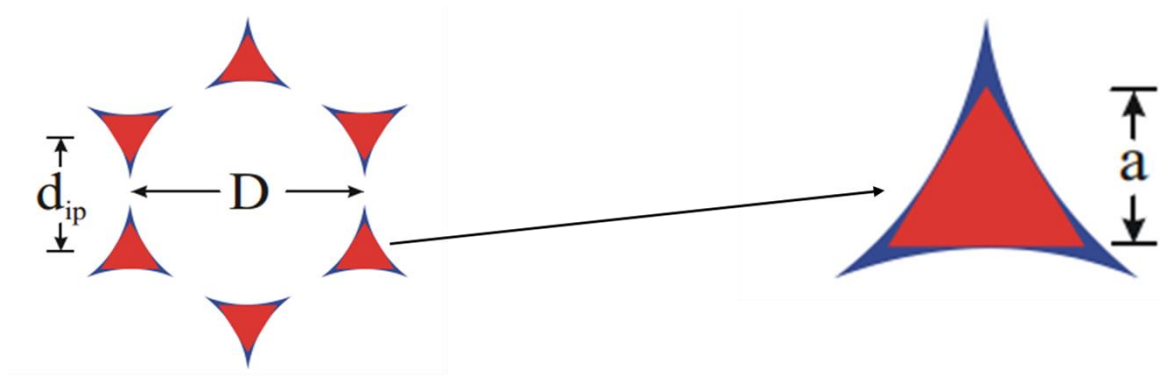


Figure 1.4. Illustration of interstitial distances and in-plane diameters of periodic particle arrays. Source: Department of Materials Science and Engineering, Northwestern University. (Accessed 03/10/2015).

Nanosphere lithography has proven to be the most preferred method for fabrication of nano-meter-scale patterns over large area. It can be used to pattern various substrates such as mica, glass, silica and copper, among others. Due to the variety of substrates, deposition materials also abound with the most common ones being polymers, proteins, noble metals and magnetic materials. Nanosphere lithography is the cheapest, easiest to use lithographic technique owing to its material general nature.

1.3 Self-Assembled Monolayers (SAMs)

1.2.1 Introduction

Self-assembled monolayers are molecular aggregates formed on a solid surface following exposure of the solid (substrate) to active amphifunctional molecules from solution or gas phase.¹⁶ Self-assembled monolayers can also be formed on liquid surfaces such as liquefied mercury and metal alloys.¹⁷ Upon their adsorption on the substrate, the molecules organize themselves through intra-molecular and inter-molecular forces. Typically SAMs contain three features; the head, tail and functional groups, as presented by **Figure 1.5**. **Figure 1.5**. Basic features of self-assembled monolayers.

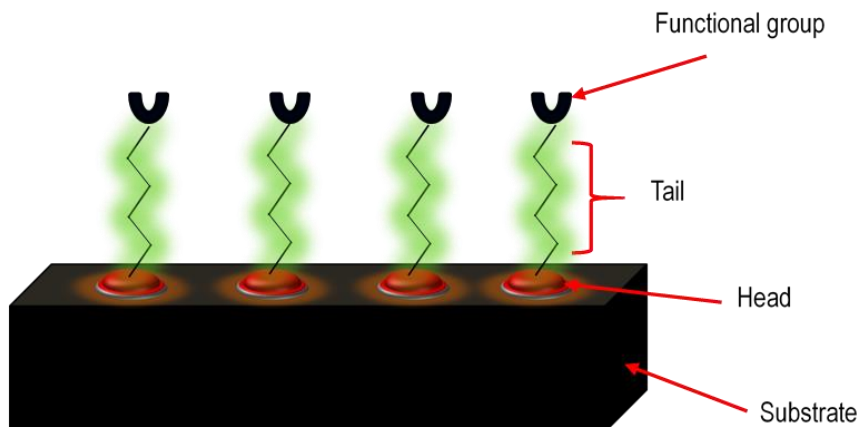


Figure 1.5. Basic features of self-assembled monolayers.

An important property of SAMs is their amphiphilic nature (one group having a strong affinity for the substrate while the other group has none or very little for the substrate), which directs one end of the molecule to the substrate's surface leaving the other

end at the air-monolayer inter-phase. The head group spontaneously adsorb on the substrate's surface through covalent or ionic bonds depending on the interacting species. Energies resulting from chemisorption are in the range of tens of kcal/mol, for example 28 kcal/mol for adsorption of thiolates on gold surfaces. This energy draws the molecules close enough for short-range intermolecular forces to be experienced.¹⁶

The tail group mostly consist of an organic moiety that bridges the head and functional groups. The magnitude of inter-chain van der Waals forces arising from the interaction of several tail groups is determined by the packing and density of the molecular aggregates.¹⁶ In the simplest case of alkyl chain interaction, van der Waals forces are ~ 8.4 kJmol⁻¹ per CH₂ group.¹⁸ At the end of the tail group lies the functional group (also known as terminal functional group). The type of functional group depends on the intended purpose of SAMs, for example -CH₃ and -COO⁻ can be used to pattern nonpolar and polar deposition materials respectively. Other commonly encountered functional groups include alcohols, esters and nitriles.¹⁸ Terminal functional group offers fundamental physical properties for engineering and surface chemistry studies. The properties also aid application of SAMs in alteration of physical and chemical properties of the surfaces e.g. in corrosion prevention and lubrication.

1.2.2 Types of Self-Assembled Monolayers

Self-assembled monolayers can be classified into several categories based on the kind of substrate and head group involved in their formation. The field of self-assemblies has witnessed an enormous growth in their classification as researchers approach it in either

a general or an individualistic perspective. In this section a more general perspective on the types of SAMs is used.

1.2.2.1 Monolayers of Fatty Acids

This type of SAMs result from adsorption of carboxylic groups of fatty acids on metal surfaces. A fatty acid is a carboxylic acid with a long aliphatic chain for example stearic acid; $\text{CH}_3(\text{CH}_2)_{16}\text{COOH}$. Gold, silver, aluminum and copper are suitable metals for developing SAMs of fatty acids. Prior to the preparation of the molecular assemblies, the metals involved are often exposed to air leading to formation of a thin oxide layer¹⁹ on their surfaces. Their reaction with the organic acids is therefore an acid-base reaction²⁰ which can take place by formation of a metal carboxylate salt such as chemisorption of the acid on a thin layer of silver oxide on silver metal. The acid can also chemisorb on some metals like aluminum through proton transfer to a lattice oxygen. Chemisorption without a proton transfer is also possible for semiconductor substrates such as silicon.¹⁹

Different metal oxides may interact differently with the oxygen atoms of the carboxylic acid. Chemisorption of n-alkanoic acid on AgO show the monolayers adopting a 26.7° tilt angle configuration unlike in Al_2O_3 surfaces where the acid molecules form perpendicular arrays on the oxide surface (*vide infra*). Silver oxide interacts symmetrically with the two oxygen atoms of the acid bound to the metal's surface but aluminum oxide form an electrostatic interaction (asymmetrically) with the deprotonated oxygen of the carboxylate resulting in different orientation of the monolayers as shown in **Figure 1.6** below.²⁰

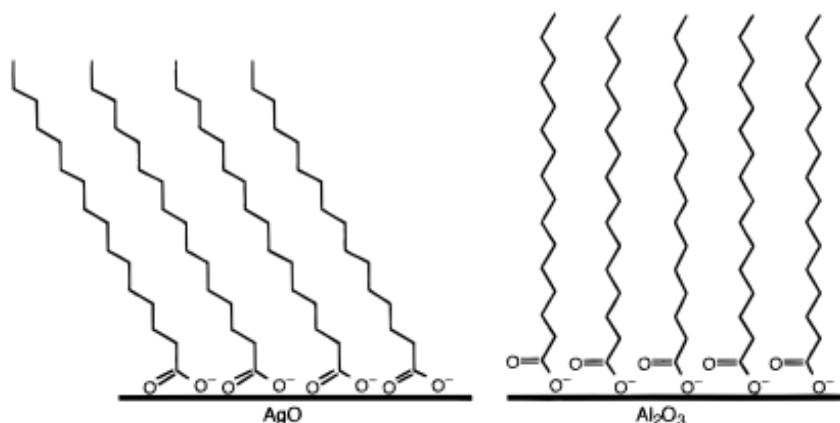


Figure 1.6. Schematic representation of fatty acid monolayers on AgO and Al₂O₃;
 Reprinted with permission from ref.²⁰ Copyright (1996) American Chemical Society.

1.2.2.2 Monolayers of Organosilicon derivatives

Organosilicon derivative monolayers include alkylchlorosilanes, alkylalkoxysilanes and alkylaminosilanes. Their exposure to hydroxylated surfaces of substrates such as silicon oxide, aluminum oxide, glass and mica lead to formation of polysiloxane on the surface's silanol groups.²⁰ This research deals with self-assemblies of octadecyltrichlorosilane (OTS) and undecenyltrichlorosilane (UTS) on silicon wafers. More information about this type of SAMs can be found in chapter 3.

It is worth noting the importance of temperature in the formation of SAMs of organosilicon derivatives. It has been found that the length of the alkyl chain influences the optimum temperature for the formation of ordered assemblies. Long alkyl chains require higher temperature than do their counterparts. This behavior is tied to the direct relationship between temperature and reaction kinetics.

Figure 1.7 illustrates arrangement of organosilicon derivative monolayers (octadecyltrichlorosilane monolayer⁵).

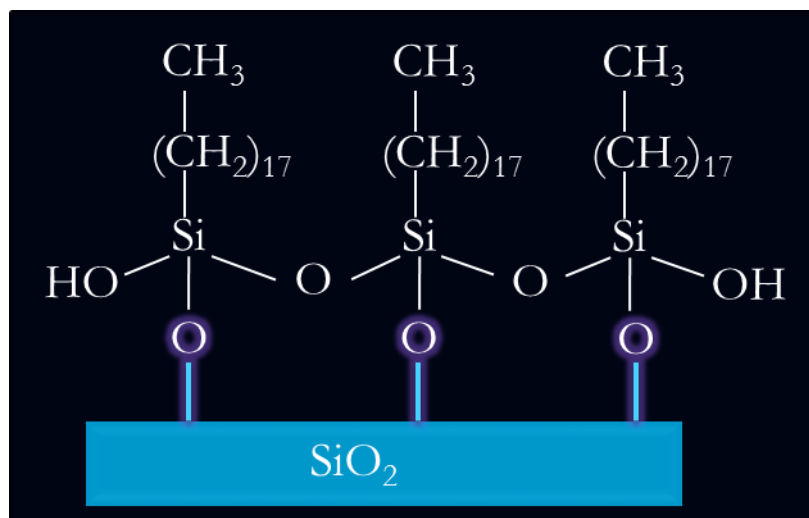


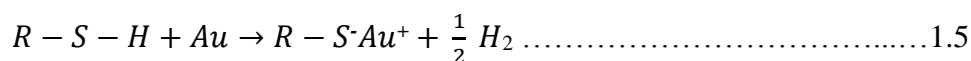
Figure 1.7. Schematic representation of OTS monolayer on Silicon wafer.

1.2.2.3 Organosulfur Monolayers on Metal surfaces

Organosulfur molecular species (thiols, sulfides and disulfides) are the most studied group of SAMs. They are formed by reaction of the terminal sulfur with transitional metals such as gold, silver, mercury etc. Long standing method for their preparation involves a 12-18 hours incubation of the cleaned metal substrates in 1-10 mM thiols/sulfides/disulfides in appropriate solvent.¹⁷The first step of the reaction is governed by reaction kinetics of the sulfur with the metal. This step takes few minutes depending on the concentration of the thiols and prevailing environmental conditions. After establishment of the sulfur-metal bond van der Waals forces and dipole-dipole²⁰

interactions within the disordered state of alkyl chains orient the tails into a more uniform manner. This is a rather slow step lasting for 12-18 hours.

Disulfides and thiolates chemisorb on gold surfaces through oxidative addition as shown in the following equations. Bonding of thiol to gold is followed by reductive elimination of hydrogen.



Formation of the RS-Au (R represents alkyl chain) has been confirmed by electrochemical, mass spectrometry, Fourier transform Infrared Spectroscopy and Raman Spectroscopy techniques.²⁰

1.4 Objectives of this Thesis

The main goal of this research is broken down into four parts; preparation of self-assembled monolayers of alkyltrichlorosilane, oxidation of vinyl group of SAMs to generate new terminal functional group, meso-scale protein patterning on surfaces of the SAMs and preparation of multilayers of SAMs. The prepared SAMs are characterized using Fourier Transform Infrared Spectroscopy, atomic force microscopy and fluorescence microscopy. Fabricated protein patterns are studied using fluorescence microscopy.

1.5 Organization of this Thesis

This thesis is divided into five chapters. The first chapter provided background information of lithographic techniques and a general account of self-assembled monolayers. Chapter two details the characterization techniques used in this research. Chapters three and four deal with preparation of self-assembled monolayers and fabrication of meso-scale protein patterns respectively. Both chapters also describe the characterization of the subject materials. Chapter five is the last chapter and its main purpose is to provide conclusions and future directions.

CHAPTER 2

INSTRUMENTATION

2.1 Fluorescence Microscopy

2.1.1 Introduction

In 1852, the British scientist Sir George G. Stokes observed that the mineral fluor spar emitted red light when illuminated with blue light. Following his observation Stokes neologized the term fluorescence from the name of the mineral; fluor spar. Stokes advanced his invention by unearthing that the wavelength of absorbed light is shorter than that of the emitted light. He referred the difference between the absorption and emission wavelengths as Stokes shift.²¹⁻²²

Though Stokes was the first to describe fluorescence scientifically, other scientists also contributed to the development of the current state of the art fluorescence microscopy. Ernst Abbe (1873) noticed that the resolution of a given objective is inversely proportional to the wavelength of the absorbed light. He discovered that resolution of light microscope is limited by diffraction. His principle (expressed as shown by equation 1.1 in the preceding chapter) became a model for improving resolution of optical microscope.²³

In 1904, August Kohler observed that some natural structures (tissues) fluoresce when illuminated with UV light, a phenomenon he reported as problematic in detection of signals by his ultraviolet microscope even though he used ultraviolet light (light of

relatively shorter wavelength ~ 275 nm).^{21,24} The first fluorescence microscope was developed by Heinrich Lehman and Stanislaus Josef Mathias von Prowazek in 1913.^{21,24} The microscope relied entirely on autofluorescence of tissues for signal production. Further advancement was made by Albert Hewett Coons and Thomas Weller in 1941 and 1954 respectively. Coons label pneumococcal anti-serum with anthracene-isocyanate but the dye faded precipitately. In 1954 Thomas Weller and Albert Coons developed an indirect technique of staining antibodies with fluorescent dyes marking the genesis of a plethora of labelling dyes.^{21,22,24} The discovery of labelling dyes widened the use of fluorescence microscopes for detection of materials that would not fluoresce on their own.

High specificity, sensitivity to a single molecule, reduced harm to live cells and high resolution has made the modern fluorescence microscope ubiquitous in life sciences.

2.1.2 Principles of Fluorescence

Fluorescence is the emission of light by certain substances (fluorophores) upon excitation from an external source of energy. The process occurs at the timescales of 10^{-9} seconds. When light of a certain wavelength is shone on a fluorophore its electron(s) can be promoted to an excited state. Excitation process; takes place in femtoseconds, is often followed by the loss of energy through vibrational relaxation (timescale $\geq 10^{-12}$ seconds) and emission of light as the electron in the excited state decays back to the ground state. The absorption and emission processes can be elucidated with the help of Jablonski diagram shown below.

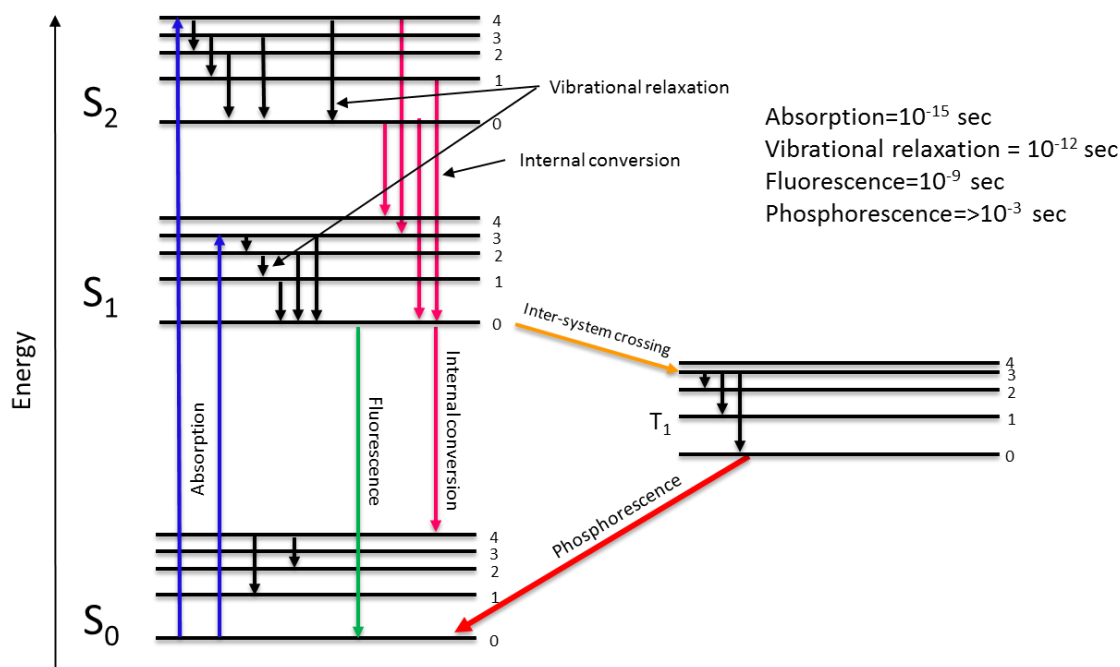


Figure 2.1. Jablonski diagram showing absorption and emission of light by a fluorophore.

In **Figure 2.1**, blue arrows indicate electronic transition to an excited state (radiative transitions), black and pink arrows represent non-radiative transitions (vibrational relaxation and internal conversions respectively) while green, orange and red arrows indicate fluorescence, transition between states with different spin multiplicity (inter-system crossing) and phosphorescence in the same order. Numbers 1-4 shows vibrational sub-levels. Singlet and triplet states are denoted by S with numerical subscripts (S_0 for singlet ground state, S_1 , S_2 for singlet excited states) and so does T for triplet state.

S_0 is the ground state, which is the state of a molecule that is not perturbed and has the lowest energy. The energy of S_1 (first excited singlet state) is less than that of S_2 (second excited singlet state). When a molecule absorbs light of appropriate wavelength (takes place at femtoseconds range²⁵), valence electron is excited to an energy state higher than the ground state. The state reached by an electron depend on the magnitude of energy of the absorbed photon given by $E = hc/\lambda$, where E is the energy, h is Planck's constant, c speed of light and λ is the wavelength of the photon. The least amount of energy needed to promote an electron to a given state is equal to the energy difference between the two states. As shown in **Figure 2.1**, an electron can move from S_0 to S_1 or S_2 (shown by blue arrows pointing upwards).

The molecule is normally unstable in the excited state and as a result it undergoes internal conversion (transitions such as S_2 to S_1) and vibrational relaxation (transfer of vibrational energy to nearby molecules), ultimately bringing the molecule to the lowest energy level of the electronic state S_1 . Vibrational relaxation and internal conversion take place at picoseconds time-scales. At the lowest level of state S_1 the molecule loses energy in form of light (fluoresce) coming back to the ground state (S_0). The emitted light always has a shorter wavelength than the wavelength of the absorbed photon because more energy is lost through intersystem crossing, internal conversion and vibrational relaxation.²²

Though formally forbidden, electronic transition from S_1 to T_1 is possible owing to their close energies' values. This transition is known as intersystem crossing (orange arrow in the figure above). At the triplet state the electron can descend to the singlet ground state S_0 by emitting light (phosphorescence). Phosphorescence takes place belatedly ($\geq 10^{-3}$ seconds) thus weakens the fluorescence signal and can worsen it in case the molecule in

the triplet state absorbs another photon that moves it to higher triplet state. Additionally, photochemical reactions can take place in the triplet state leading to irreversible bleaching and photo-toxicity.

Bleaching is the permanent fading of fluorescence signal. This phenomenon majorly occur due to intersystem crossing. Emission of energy (phosphorescence) in triplet state is delayed which would expose the molecule to any reactive species. The delayed signal will not be recorded because of huge time difference between fluorescence and phosphorescence. The energy in triplet state can also excite any oxygen molecule in the milieu thereby rejuvenating reactions of oxygen with organic molecules. The reactions would cause permanent fading of the fluorescence signal. The reactive excited oxygen also has ability to interfere with bioactivity of living cells (photo-toxicity).²² Bleaching can be minimized by exposing the fluorophore with light for very short periods (this reduces the number of excitation-emission a molecule has to undergo) and storing samples in the dark to avoid any excitation from background lightings.

2.1.3 Fluorescence Microscope

The modern fluorescence microscope employ epi-illumination technique whereby the microscope's objective images, magnifies and illuminates the sample. The epi-illumination mode minimizes the amount of exciting light (normally reflected off the specimen) that has to be blocked in the return light. However the method requires a medium (dichroic mirror) through which the excitation and emission lights can be separated. A dichroic mirror is often used alongside two filters (emission and excitation filters).²² **Figure 2.2** below illustrates the basic working principle of a fluorescence microscope.

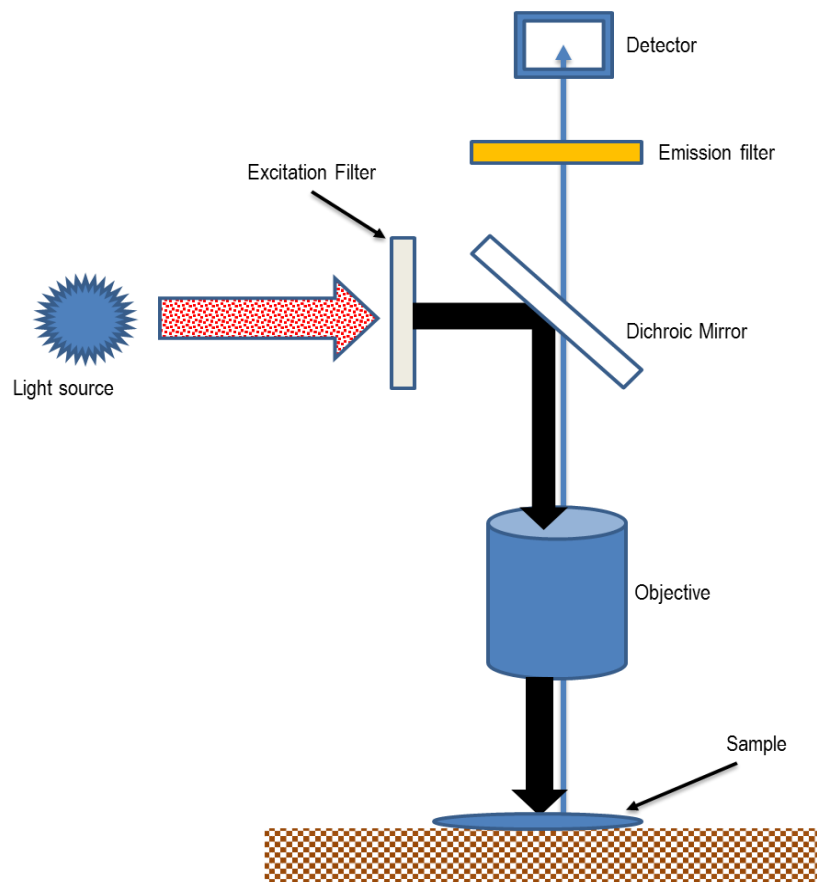


Figure 2.2. Working principle of fluorescence microscope.

The source of light must be strong enough to counteract the low collection efficiency of the microscope, ultimately increasing the number of photons that reach the eye. Commonly used light source is the arc lamp made up of either mercury or xenon. Though the lamp of interest depends on the sample under experimentation, xenon lamps are preferred over the former. Unlike mercury, xenon lamps cover a wide range of wavelengths; UV, Visible and near infrared. On the other hand mercury lamps produce brighter images, a fact attributed to its high mean luminous flux per surface area.^{22, 26}

To excite the sample light from the lamp is directed to an excitation filter which screens off unwanted wavelengths. The sought after light wavelength passes through the filter and on striking the dichroic mirror it is reflected through the objective to the specimen. After absorbing a photon of appropriate energy the sample fluoresces. The emitted light from the sample subsequently passes through the objective and the dichroic mirror to the emission filter. The emission filter blocks any excitation wavelength hence the detector receives signal from the specimen.²⁶

2.1.4 Conclusion

Fluorescence microscopy is undoubtedly one of the most powerful imaging techniques used in nanotechnology. The staining process makes it possible to obtain images of substances that do not fluoresce on their own. The use of fluorescein isothiocyanate dye to label lysozyme, and red and infrared dyes to dye the background are testaments to that fact. Minimizing times for light exposure to samples would help in reducing photobleaching. Further sophisticated modalities such as recovery of fluorescence after photo-bleaching, total internal reflection fluorescence; just to mention a few, signals that improvement of fluorescence microscopy is far from over.

2.2 Fourier Transform Infrared Spectroscopy (FTIR)

2.2.1 Introduction

The infrared region exist between the visible and microwave regions of the electromagnetic spectrum. **Figure 2.3**, illustrates the range of wavelengths/frequencies of infrared radiation relative to other waves/radiations of the electromagnetic spectrum.

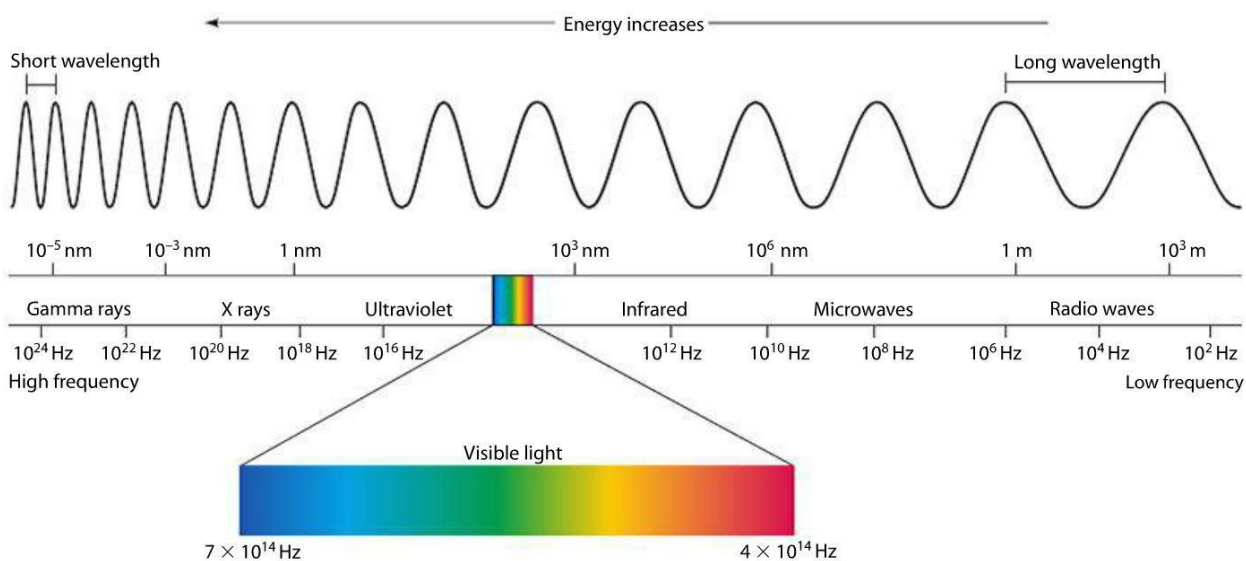


Figure 2.3. Electromagnetic spectrum. Source: Natural science Inc1 with None at Western Governors University. Online: (Accessed 1/28/2015).

Infrared (IR) spectrum is divided into three regions based on the wavelength/frequency, viz; near-IR, mid-IR and far-IR. Near-IR extends to the visible region and it provides information for high frequency ($1700\text{-}4000\text{ cm}^{-1}$) absorption bands such as overtone, combination and strong bonds. Before the advent of Fourier transform spectrometer mid-IR ($670\text{-}4000\text{ cm}^{-1}$) was chiefly used for qualitative analysis and

structural determination of organic substances. Restriction to mid-IR wavelength is due to relatively low detection limits and signal to noise ratios of dispersive type spectrometers; the prime instruments at that time. In the present time mid-IR is not only useful for qualitative purposes but also as a tool for quantitative analysis of complex liquid, solid or gaseous mixtures. The far-IR ($\leq 650 \text{ cm}^{-1}$) is utilized in qualitative analysis of inorganic/organometallic compounds.²⁷

When a molecule is exposed to IR radiation, vibrational excitations of its bonds take place. Photons absorbed by the molecule are characteristic of the functional group or bonds that vibrate. Chemists make use of the unique vibrational frequencies of individual bonds to predict the functional group and in some cases structure of the molecule.²⁷

Chemical bonds behave as harmonic oscillators and therefore Hooke's law is particularly useful in determining their vibrational frequencies. Hooke's law relate the frequency and the mass of the atoms constituting the bond according to equation 2.2.1

$$\nu = \frac{1}{2\pi c} \sqrt{\frac{k}{\mu}} \dots\dots\dots 2.1$$

where c is speed of light, ν is vibrational frequency (in wavenumbers), k is force constant and μ reduced mass ($\mu = \frac{m_1 m_2}{m_1 + m_2}$, where m_1 and m_2 are masses of the two atoms that form up the bond under consideration).

It is discernible from Equation 2.1 that strong bonds and bonds between lighter atoms vibrate at higher frequencies than their counterparts. The equation does not account for anharmonicity terms (repulsion and attraction of electron clouds during bond vibration) of the vibration. However it is very much accurate for vibrational frequencies resulting

from transition from ground state to the first quantum level. The effect of anharmonicity terms become significant during excitation to higher energy states (overtone), thus adjustment to account for their effect should be considered. Anharmonicity causes deviation from infrared radiation selection rule that states that the frequency of vibration is quantized.²⁸⁻²⁹

The number of vibrational modes of a given molecule depend on the geometry (whether linear or non-linear) and the number of atoms making up the molecule. These modes are determined from the equations below

$$\text{Number of normal modes} = 3N - 6 \text{ (nonlinear)} \dots\dots\dots 2.2$$

$$\text{Number of normal modes} = 3N - 5 \text{ (linear)} \dots\dots\dots 2.3$$

where N signifies the number of atoms in a given molecule.²⁹

Infrared absorption requires that the dipole moment of the molecule changes during its vibration or rotation. Alternating electric field of the radiation interact with the fluctuating dipole moment yielding a net change in amplitude in one of the motions of the molecule. The molecule absorbs a frequency of the IR radiation that matches its natural vibration frequency resulting in a change in the said amplitude. Symmetric bonds with similar groups on both ends, and homo-nuclear species do not absorb IR radiation. Representatives of symmetric bonds and homonuclear molecules include C=C bond in 2, 3-dimethyl-2-butene and oxygen (O₂) respectively.

2.2.2 The Fourier Transform Infrared (FT-IR) Spectrometer

The FT-IR spectrometer was invented in the 1980s. It is regarded as the most convenient and effective instrument for IR analysis. The instrument employs an interferometer where all absorbed frequencies are simultaneously measured and subjected to the mathematical process of Fourier transformation to obtain a spectrum. Earlier instruments (dispersive type spectrophotometers) relied on diffraction gratings or prisms for separation of IR frequencies.^{27, 20}The general working principle of Fourier type spectrometers is illustrated in **Figure 2.4**.

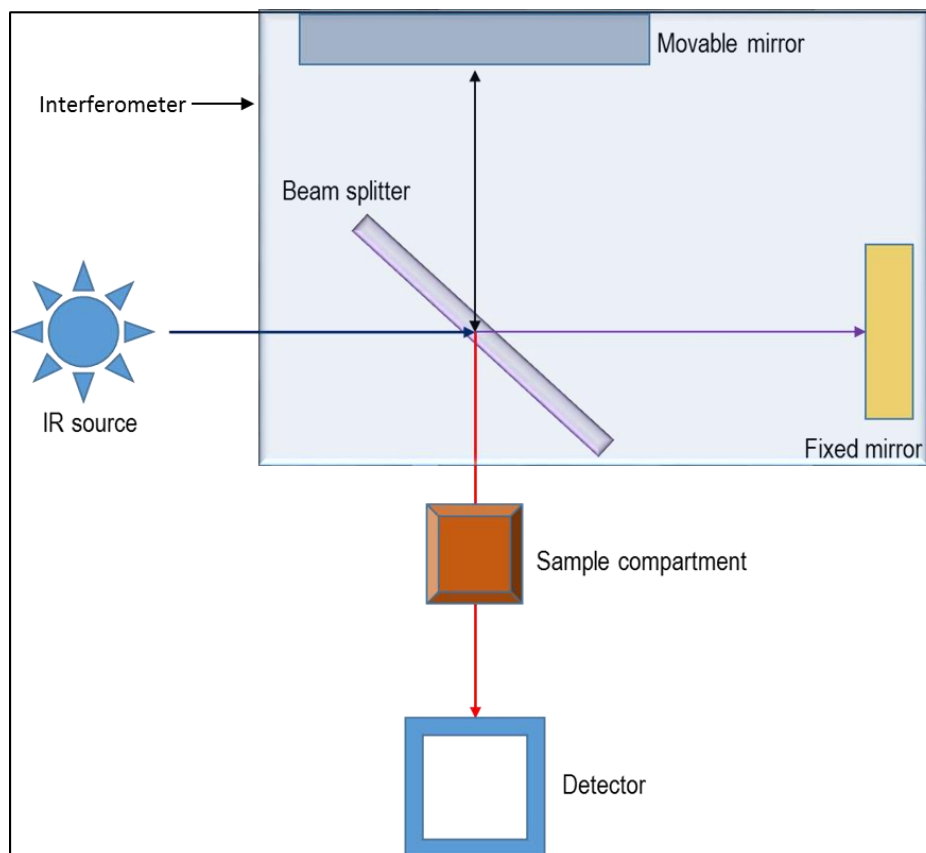


Figure 2.4. Working principle of single-beam FT-IR spectrometer.

On its way to the detector, the infrared radiation from the source (silicon carbide rod is the commonly used IR source for FTIR spectrometers) is subjected to several reflections. The beam of radiation from the source is directed to the interferometer where it encounters the beam-splitter which theoretically halves it and direct one half to the movable mirror and the other half to the fixed mirror. Both mirrors subsequently reflect the beams back to the beam splitter where recombination and interference take place based on the appropriateness of their phase difference. The beam splitter then reflects half of each of the light intensities (25 % each of the original incident radiation) through the sample in the sample compartment to the detector. The constant shifting of the movable mirror is instrumental for interference of the beams of light upon their convergence at the beam splitter. It is from this interference that an interferogram is obtained. The interferogram is then send to a connected computer which subjects it to Fourier transformations and finally produce an infrared spectrum.³⁰

2.2.3 Interpretation of infrared spectrum

Infrared spectrum is a plot of percent transmittance/absorbance against frequency (wavenumbers). Transmittance is defined as the fraction of the incident radiation that passes through the sample.

$$Transmittance, T = \frac{P}{P_o} \dots\dots\dots 2.4$$

where P and Po represent radiation that passes through the sample and incident/original radiation respectively. Percent transmittance is obtained by multiplying T

by 100. The relationship between transmittance and absorbance, A is given by the equation below.

$$A = \log\left(\frac{P_0}{P}\right) = -\log T \dots\dots\dots 2.5$$

Absorbance is particularly useful in quantitative analysis where Beer-Lambert's law expression is used.

$$\text{Beer - Lambert law: } A = \epsilon bc \dots\dots\dots 2.6$$

where ϵ is molar absorptivity, b is path length and c is concentration of the sample

A typical infrared spectrum (% transmittance versus wavenumbers) is divided into two regions; group and fingerprint regions. The group frequencies region range from 3600 to 1250 cm^{-1} and the fingerprint region include frequencies below 1250 cm^{-1} . Group frequencies provide information about existence of functional groups such as C=O, O-H and C=C in the sample while the fingerprint region provide the identity of the compound.³¹

2.2.4 Conclusion

Infrared spectroscopy is a great characterization technique for any analytical laboratory. Unlike nuclear magnetic resonance (NMR) spectroscopy that is restricted to atoms with odd mass or proton number, FT-IR can be used to effectively study any bond vibration as long as there is a net dipole change during the vibration. The introduction of Fourier transform further favored the use of IR spectroscopy in sample analysis. Interferometer of FT-IR spectrometer measures all infrared frequencies simultaneously rather than individual frequencies at a time, as in the case of IR spectrometers. Additionally

the detectors used are very sensitive and the instrument is internally calibrated (HeNe laser is used for internal calibration). Dispersive type instruments require manual calibration by the user.³²

2.3 Atomic Force Microscopy (AFM)

2.3.1 Introduction

Atomic force microscopy falls under a class of imaging techniques called scanning probe microscopy (SPM). Scanning probe microscopy was introduced in 1982 to provide topographical properties of materials.³³ The technique works by scanning surfaces of samples with a sharp object (probe) whereby the interaction of the tip of the probe with the sample is converted into an interpretable image. Besides AFM, Scanning tunneling microscopy (STM) and stylus profilometer (SP) are among other notable forms of SPM. The earlier was invented by Binnig and Rohrer in 1982. The pair was awarded a Nobel Prize for Physics in 1986 for their invention.³⁴ Though SPM was effective in imaging conductors, attempts to use it to obtain the morphology of insulators were futile as it relies on a tunneling current generated between the probe and the sample. Stylus profilometer gauges the roughness of the surface resulting from up and down movement of its stylus as it scans the sample under observation.³⁶

Prior to the invention of atomic force microscope researchers were puzzled on how to obtain images of insulators without relying on the coating of such surfaces with metals. While on leave from IBM-Zurich research, Gerd Binnig³⁷ reasoned that it could be possible to obtain images of materials by applying an ultra-small force in lieu of the tunneling current used in STM. He shared his hypothesis with Calvin Quate and

Christopher Gerber and the trio successfully developed the atomic force microscope which is capable of imaging insulators, semiconductors and good electrical conductors.³⁴ They designed the microscope in such a way that a soft cantilever with a sharp tip (conducting or non-conducting) can be moved over the sample and the deflection and/or bending of the cantilever is converted into an analogue image (see section 3.2 for details).³⁷ The first crop of AFMs used handmade gold cantilevers with diamond tips which were later replaced with microfabricated silicon nitride (Si_3N_4) tips.³⁷ Upon its inception the use of atomic force microscope quickly spread across the natural sciences.

2.3.2 Basic working principle of atomic force microscope

Atomic force microscope has three modes of operation which include contact, tapping and non-contact modes. The contact mode is the most reliable in terms of reproducibility of data. The basic working principle of contact mode is illustrated in **Figure 2.5**.

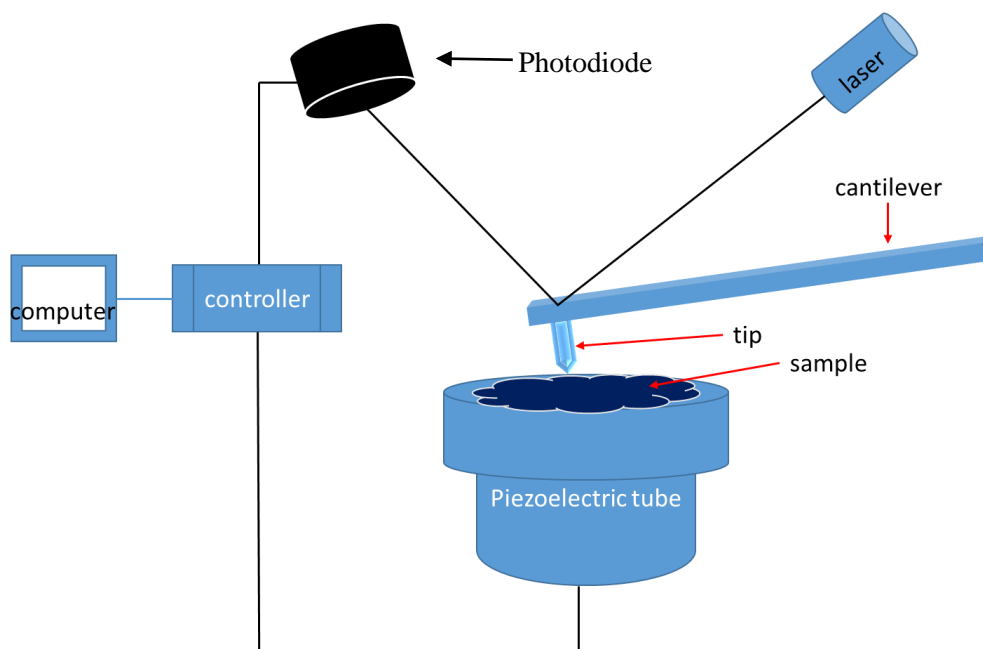


Figure 2.5. Illustration of working principle of atomic force microscope.

Basic components of AFM are shown in the figure above. Movement of the tip of the cantilever across the surface of the sample is in principle, the starting point of the working of the microscope. The tip is brought in contact with the sample where the piezoelectric actuator either moves the sample against the tip or moves the tip across the sample.³⁵ As the tip scans the surface it encounters several forces that send the cantilever in an up and down, and in some cases sideways' undulation or bending. When the tip is in contact with the sample the electron clouds of the atom at the tip and atoms making up the sample interact with each other producing a repulsive force. The repulsive force pushes the tip up and as the interatomic distances increases another attractive force sets in causing the tip to move down or towards the sample again.³⁸ The forces produced between the tip and

the sample are in the range of 10^{-11} to 10^{-6} N which falls within the orders of interatomic forces (10^{-9} N).³⁹

The deflection of the cantilever reflects the laser beam shone on the back of the cantilever-tip assembly to the photodiode.³⁵The reflected laser beam keep shifting its position on the surface of the photodiode with respect to the displacement of the cantilever. The photodiode finally transmit the signal through the controllers to the computer where a topographical image is obtained.³⁸

Resolution of atomic force microscope is determined by the radius of the tip of its cantilever. The smaller the tip's radius the higher the resolution. Most AFM instruments have a lateral resolution of 1.0-2.0 nm.³⁸

2.3.3 Conclusion

Atomic force microscope did not only enable researchers to obtain images of non-conducting and conducting materials but it can also be used in diverse environmental conditions such as dry/air or wet/water conditions.³⁵ Further reduction of the size of the tip increased its resolution making it superior among the scanning probe microscopes and a tool of choice for studying surface properties of materials. Its atomic scale resolution in three dimension³⁵ made it possible to study growth of self-assembled monolayers on substrates and imaging of biological macromolecules.

CHAPTER 3

PREPARATION AND CHARACTERIZATION OF SELF ASSEMBLED MONOLAYERS

3.1 Introduction

Different types of self-assembled monolayers have been discussed in chapter one. Thickness of SAMs ranges between 1-3 nm¹⁷ and therefore they are nanostructures. These molecules are very important in the field of nanotechnology with innumerable cross-disciplinary applications. One unique property of SAMs is that their terminal group can be modified through chemical means. The modification produces new terminal functional groups opening varied opportunities for studying their physical-organic chemistry with different types of biomolecules or synthetic compounds.

The widespread use of SAMs in nano-science is attributed to their ease in preparation using unsophisticated instruments under easily achievable environmental conditions. In the nascence of studies of SAMs, researchers focused largely on preparation of molecular assemblies of organosulfur compounds on metals' (mainly gold and silver) surfaces through solution and gaseous phases. Solution and gas phase preparation methods are still used and they are the two methods employed in our laboratory. **Figure 3.1**, illustrates preparation of SAMs via solution phase.

The number of different types of molecular assemblies under research is ever on the rise due to introduction of new substrates. Study of SAMs is motivated by varying needs for diverse surfaces for tailoring special molecules with great research and technological merits. Self-assembled monolayers studied in this research are those of alkyltrichlorosilanes on silicon wafers, specifically octadecyltrichlorosilane (OTS) and undecenytrichlorosilane (UTS) on Si(100) surfaces (molecular structures shown in **Figure 3.2**).

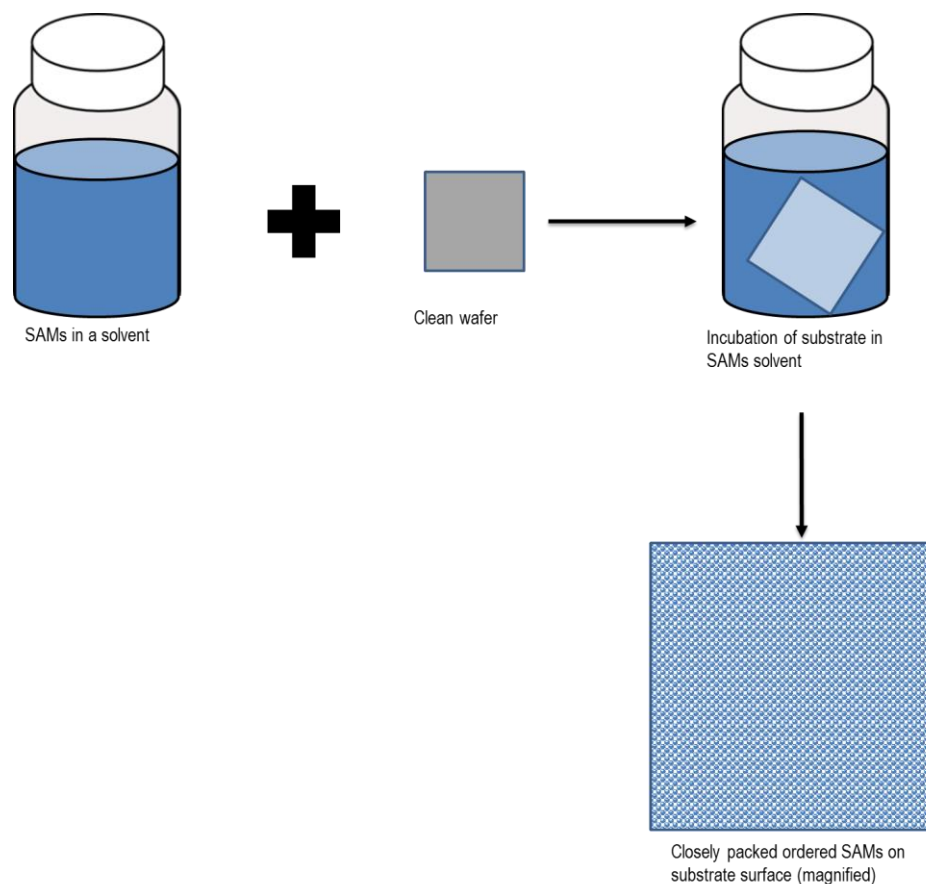


Figure 3.1. Schematic representation of growth of SAMs in solution.

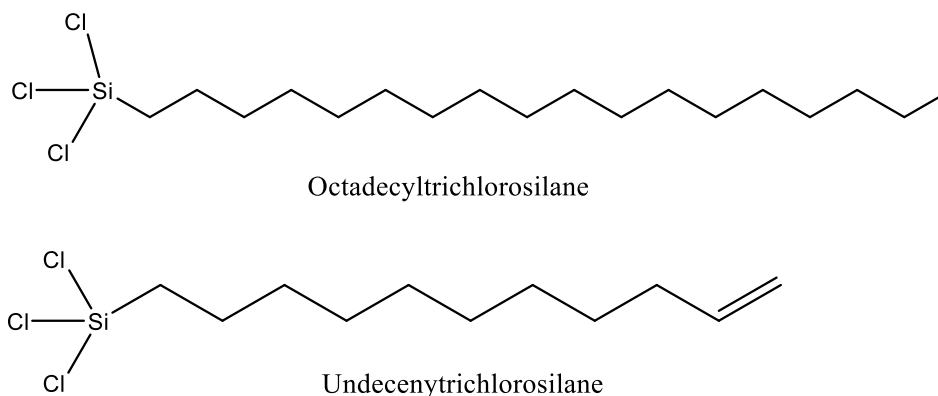


Figure 3.2. Structure of self-assembled monolayers used in this research.

The success in SAMs' studies is linked to the advent of new powerful and diverse tools for characterizing them. As discussed in the preceding chapter Fourier-Transform Infrared Spectroscopy, atomic force microscopy and fluorescence microscopy are the main analytical tools for characterizing SAMs used in this research. Other characterization techniques include ellipsometry, x-ray photoelectron spectroscopy, scanning probe measurements¹⁸ and polarized infrared external reflectance spectroscopy (PIERS).⁴⁰

3.2 Experimental: To prepare and characterize self-assembled monolayers

3.2.1 Materials

Silicon (100) wafers (p-type virgin test grade) were obtained from University wafers while octadecyltrichlorosilane, 95% (nitrogen flushed) and undecenyltrichlorosilane were purchased from Acros Organics, New Jersey, U.S.A., and Gelest Inc., 11 Steel Rd. East, Morrisville PA., respectively. The toluene used as a solvent for SAMs was spectrophotometric grade 99+% from Acros Organics. Sulfuric acid

(certified ACS plus) and hydrogen peroxide (30% in water) were from Fisher Scientific, Fair Lawn, New Jersey 07410, U.S.A. The nanospheres used as lithographic masks were 900 nm polystyrene (solids 10.11%) and 500 nm silicon (10 mg/ml), and were bought from Bangs Laboratories, Inc., and NanoComposix 4878 Ronson Ct, San Diego, CA 92111 respectively. Millipore water (18.2 MΩ.cm at 25 °C) was used in the entire preparation process. Hydrazine (anhydrous 98%) was bought from Sigma Aldrich Co. LLC.

Eastern Kentucky University, Chemistry Department provided us with sodium carbonate, potassium permanganate, sodium periodate, 99% and hydrochloric acid. All chemicals were used without further purification. After use, octadecyltrichlorosilane and undecenytrichlorosilane were stored in a desiccator (room temperature) for future experiments. Hydrogen peroxide, polystyrene and silicon nanospheres were stored in a refrigerator at 2-8 °C to minimize decomposition. Other chemicals were stored in their respective containers and storage cabinets at room temperature conditions.

3.2.2 Procedure I: Preparation of SAMs

Silicon (100) wafers were cut into $1 \times 1 \text{ cm}^2$ pieces using a diamond pen and rinsed with deionized water. The wafers were then dried with a stream of air and boiled in a piranha solution (30 % hydrogen peroxide (H_2O_2) and 98 % sulfuric acid (H_2SO_4) in the ratio 1:2) for 20 minutes at 120-125°C. After heating the solution is removed from heating plate and cooled to room temperature. The reason for heating the wafers in the piranha solution (strongly corrosive and oxidizing agent) is to remove organic impurities^{18, 41} that would otherwise impair growth of SAMs on the surface. This process also aids hydroxylation (growth of a thin oxide layer of Si-OH groups) of Si (100) surfaces readying

them for bonding with active organic molecules.¹⁸The grown oxide layer makes the wafers' surfaces hydrophilic.

Cooled substrates were removed from piranha solution, rinsed with Millipore water and dried with a flow of air. Dry wafers were incubated in 5×10^{-3} M OTS in toluene and incubated for 12 hours. During the incubation period surface-bound water on the wafer hydrolyzes the Si-Cl bonds to form Silanol (Si-OH) groups. The silanol groups undergo condensation reactions to produce Si-O-Si bonds marking the chemisorption of the molecules on the wafer or binding with adjacent alkylsilane molecule.

Mass and volume measurements for preparation of 5×10^{-3} M solutions of OTS was done according to equations 3.1. Volume of toluene (solvent) used was 15 ml.

$$\text{Vol of OTS} = 0.015 \text{ L} \times 0.005 \frac{\text{Mol}}{\text{L}} \times 387.93 \frac{\text{g}}{\text{mol}} \div 0.984 \frac{\text{g}}{\text{ml}} = 0.030 \text{ ml} \dots 3.1$$

The incubation solution was prepared by measuring 15 ml of toluene into separate vials. Then 30 μL of OTS was accurately measured using microliter pipettes and dissolved in the toluene. **Figure 3.3** illustrates formation of OTS on Si (100) wafer.

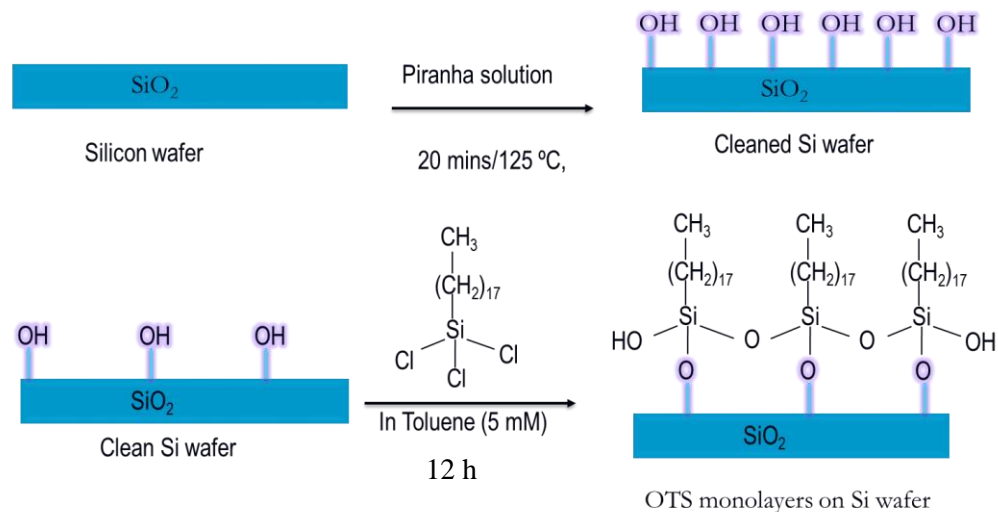


Figure 3.3. Illustration of formation of octadecyltrichlorosilane on Silicon surface.

After 12 hours silicon wafers in the OTS solutions were removed, rinsed with toluene and then wiped gently with a kimwipe. Wiping is necessary for removal of molecules that are not chemisorbed on the substrate. The prepared OTS monolayers were taken to University of Kentucky for characterization. OTS monolayers grown on silicon wafers are stable against detergents, organic solvents. They can also withstand acidic conditions but deteriorate in basic solutions. Moreover they are thermally stable below 100°C⁴².

3.2.3 Characterization of octadecyltrichlorosilane SAMs

Our OTS monolayers were characterized at University of Kentucky using atomic force microscope (Picoscan 3000; Angilent Technologies) and Fourier Transform Infrared spectrometer (Varian Exalibur 3100) because we did not have these instruments in our lab.

Results obtained are presented in **Figure 3.4**. The uniform AFM topographical image depicts homogeneous and densely packed monolayers on the substrate. AFM topographical and phase images show that octadecyltrichlorosilane molecules formed a featureless and homogeneous film on the wafer's surface. The highly oriented and densely packed OTS film was very flat. The image shows the height variation was less than 5 nm over the AFM scanner's range ($90 \times 90 \mu\text{m}^2$). The average thickness of OTS-SAM from AFM measurements was found to be ~ 2.4 nm. The same thickness was obtained from ellipsometry¹⁸ and x-ray reflectivity studies⁴³⁻⁴⁴.

Theoretical calculations of length of a stretched n-alkane molecule can be obtained as given by equation 3.2.

$$l = ((n - 1) \times a) + b \dots\dots\dots 3.2$$

$$l = ((18 - 1) \times 0.1265 \text{ nm}) + 0.15 \text{ nm})$$

$$l = 2.3 \text{ nm}$$

where l is the length of the alkyl chain including the terminal $-CH_3$ group, n is the number of carbon atoms, a is $C - C$ bond length in all-trans configuration and b is the bond length from the methyl group.⁴³

FT-IR also confirmed presence of OTS film on Si (100)/SiO₂ exterior. Peaks at 2918 cm^{-1} and 2850 cm^{-1} are due to sp^3 C-H asymmetric and symmetric stretches respectively. Intensity of IR spectra increase with increase in the number of atoms giving rise to it.⁴⁵ Each OTS has one methyl group and seventeen methylene groups and that is why the sp^3 C-H stretches have low intensity in the spectrum. The high intensity peaks at 2918 cm^{-1} and 2850 cm^{-1} are characteristic of sp^2 C-H asymmetric and symmetric stretches respectively.

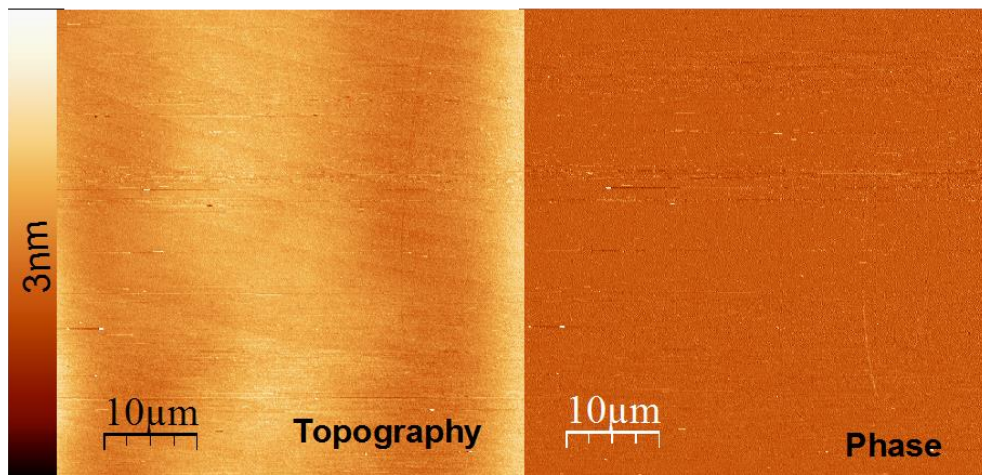


Figure 3.4. AFM Topography and Phase images of OTS in $50 \times 50 \mu\text{m}^2$ area.

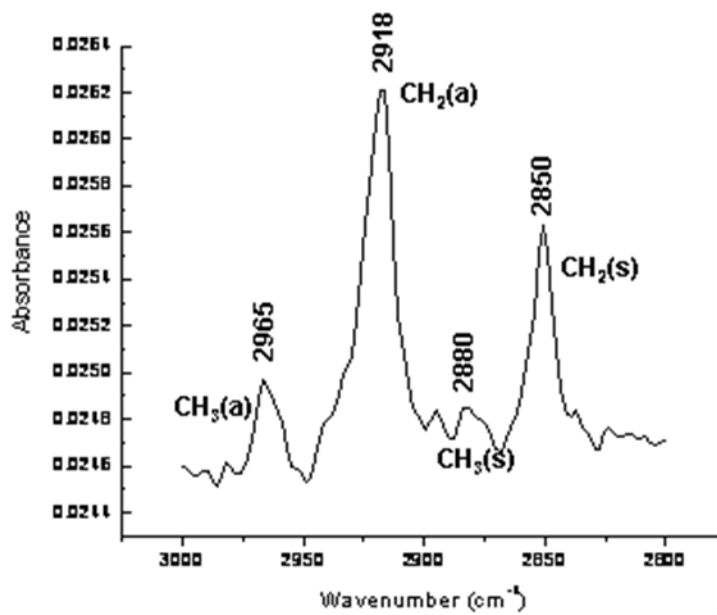


Figure 3.5. FT-IR spectra of OTS monolayer on silicon surface.

3.2.4 Procedure II: Preparation and Oxidation of UTS SAMs

Procedure used to grow UTS self-assemblies on Si (100) is the same as that used to prepare OTS (section 3.2.2). Equation 3.3 shows volume calculations used.

$$\begin{aligned} \text{Vol of UTS} &= 0.015 \text{ L} \times 0.005 \frac{\text{Mol}}{\text{L}} \times \left(287.73 \frac{\text{g}}{\text{mol}} \right) \div 1.04 \frac{\text{g}}{\text{ml}} \\ &= 0.02075 \text{ ml} \dots\dots\dots 3.3 \end{aligned}$$

The purpose of oxidizing UTS is to modify the terminal alkene (non-polar) group into a carboxylic acid. The polar -COOH group would then be used to fabricate lysozyme (a polar protein) patterns on a later stage.

Oxidation solution for converting the vinyl group of UTS to carboxylic group was prepared by dissolving accurately weighed 13.25 mg of potassium permanganate (KMnO₄), 10.69 mg of sodium periodate (NaIO₄) and 66.24 mg of sodium carbonate (Na₂CO₃) in 25 ml Millipore water in a vial. These measurements correspond to concentrations of 5.0 × 10⁻⁴ M, 0.02 M and 0.025 M respectively (see equations 3.4, 3.5, 3.6 for mass calculations). The pH of solution was measured using a pH paper. KMnO₄ and NaIO₄ oxidize the C=C to -COOH, while Na₂CO₃ was used as a buffer (to maintain the pH of the solution at 8). A buffer was necessary at this point because alkylsiloxane monolayers are fairly stable in organic solvents, water and acid but unstable in prolonged basic conditions.⁴¹ UTS-substrates were dipped into the oxidation solution and stored in a vacuum oven at 40 °C for 24 hours. The temperature is high enough for oxidation of the vinyl group but not too high for decomposition of the monolayers.

After oxidation the sample was rinsed with Millipore water. The surface of the wafer appeared hydrophilic which imply formation of polar groups. To remove KMnO_4 and other oxidant residues the SAMs were rinsed with hydrazine for one minute. This is followed by rinsing with Millipore water again. Finally the sample was rinsed with 10% hydrochloric acid and dried with a flow of air. At this point the oxidized layer is ready for characterization. A schematic representation of conversion of alkene group to carboxylic acid is shown in **Figure 3.6**.

$$\text{Mass of KMnO}_4 = (0.0005 \frac{\text{mol}}{\text{L}} \times 0.025 \text{ L} \times 158.03 \frac{\text{g}}{\text{Mol}} = 0.0020 \text{ g} \dots 3.4$$

$$\text{Mass of NaIO}_4 = \left(0.02 \frac{\text{mol}}{\text{L}} \times 0.025 \text{ L}\right) \times 213.89 \frac{\text{g}}{\text{Mol}} = 0.1069 \text{ g} \dots 3.5$$

$$\text{Mass of Na}_2\text{CO}_3 \left(0.025 \frac{\text{mol}}{\text{L}} \times 0.025 \text{ L} \times 105.99 \frac{\text{g}}{\text{Mol}} = 0.066 \text{ g} \dots 3.6$$

Directly synthesizing hydrophilic monolayers with a carboxylic acid moiety on silicon surface has proved to be challenging because both ends can interact with the thin silicon oxide layer to produce mixed surface properties.⁴⁶ As such it was necessary to develop UTS and then oxidize it at a later stage. Oxidized UTS is abbreviated UTSox in this thesis.

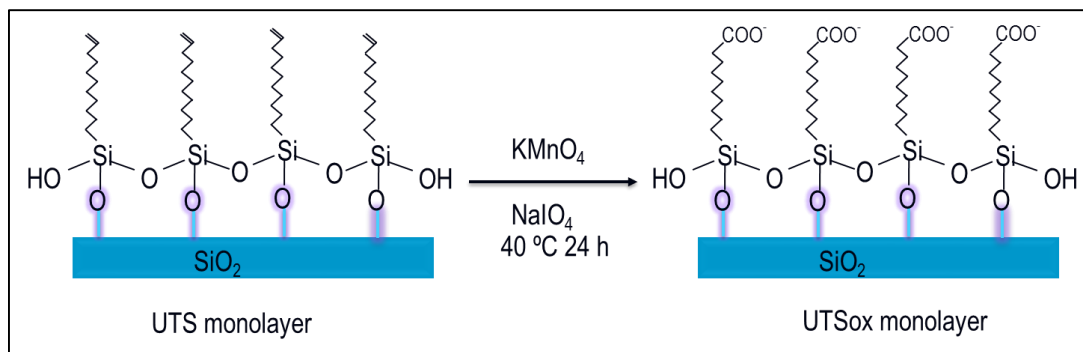


Figure 3.6. Illustration of surface oxidation of UTS monolayer.

3.2.5 Characterization of UTSox

FT-IR characterization of UTSox was performed at University of Kentucky and the results are presented **Figure 3.7** (spectrometer used has been stated elsewhere in this paper).

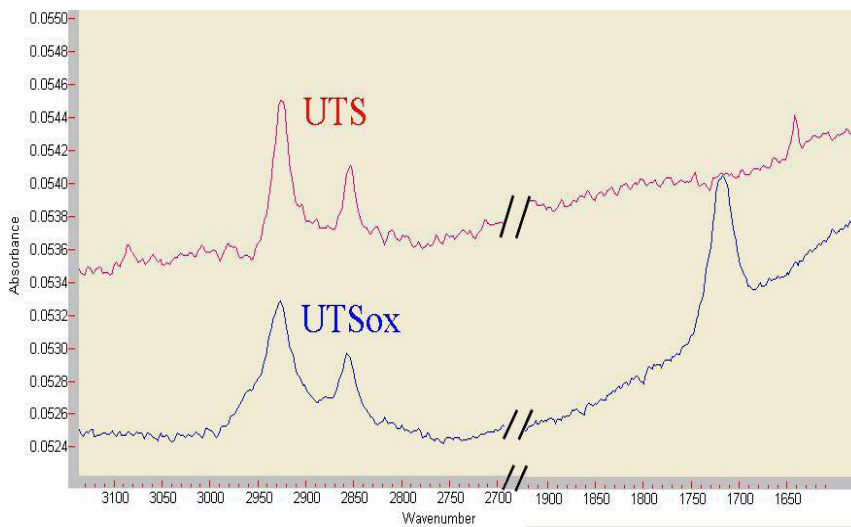


Figure 3.7. Brewster angle IR spectra of UTS (red) and UTSox (blue).

The FT-IR spectrum shows a dramatic change in surface properties of the monolayer. This is because of the new high intensity peak centered at $\sim 1710\text{ cm}^{-1}$ which is characteristic of $-\text{CO}_2\text{H}$. The mechanism for conversion is shown in **Figure 3.8**.

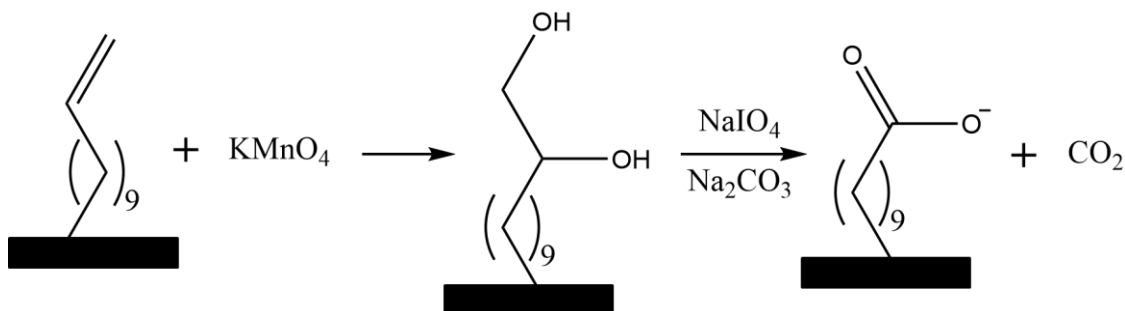


Figure 3.8. Scheme for conversion of vinyl group to carboxylic group

In our lab we characterized UTSox using fluorescence microscope (Nikon 80i microscope). UTSox does not fluoresce upon excitation with fluorescent light and as such we had to tag it with 1-pyrenyldiazomethane (PDAM), an effective fluorophore.

UTSox monolayers were dipped into a solution of 3 mM PDAM in methanol and incubated for 12 hours at room temperature. PDAM react with carboxylic acid to as illustrated in **Figure 3.9**.

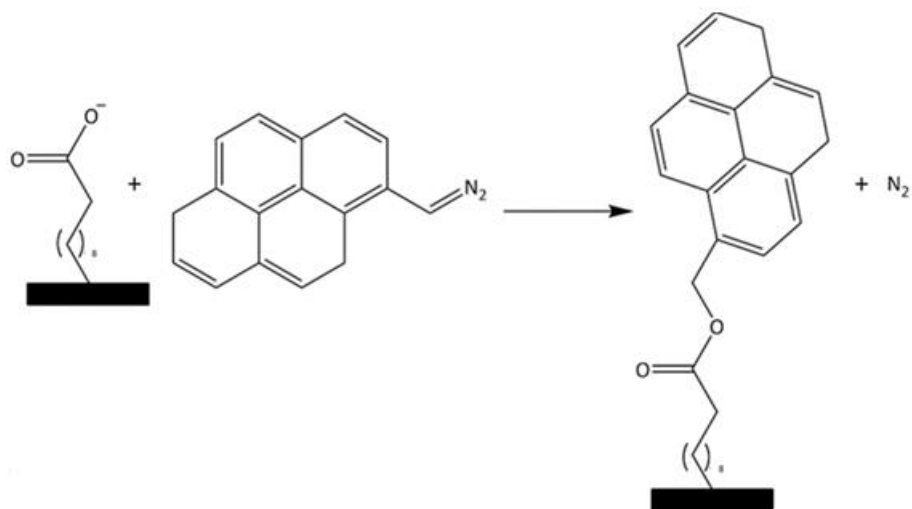


Figure 3.9. Illustration of staining UTSox with PDAM.

3.2.6 Conclusion

We have demonstrated the formation of self-assembled monolayers of alkyltrichlorosilanes on Si(100) wafers. Results from atomic force microscope images revealed formation of uniform films of OTS. The SAMs had the same height as topography image shows. Phase image shows uniformity of surface properties. This means the surface of the wafer was primarily covered by OTS. We were also able to successfully prepare undecenyltrichlorosilane monolayers and further oxidizing them to UTSox as confirmed by FTIR and fluorescence images.

The stability and compact nature of self-assembled monolayers once formed on the surfaces of materials make them useful in wear and corrosion prevention. Additionally these molecular assemblies are biocompatible.²⁰ As a result they can be used as biosensors to probe presence of biomolecules. It is for this reason that we have used UTSox SAMs to pattern lysozyme protein.

CHAPTER 4

FABRICATION AND CHARACTERIZATION OF PROTEIN PATTERNS BASED ON NANOSPHERE LITHOGRAPHY

4.1 Introduction

Technological advancement is motivated by an urge to improve the quality of man life. With a burgeoning global population and emergence of new diseases, the scientific community has to devise novel strategies for combating the dilemma of epidemics. An understanding of how biological molecules such as proteins interact with man-made surfaces is key to finding a solution to the extant and emerging life-style associated health problems. Proteins are important biomolecules involved in catalysis, force generation, mechanical support, signaling and sensing within the body. They can be incorporated into nano-devices to develop highly efficient biosensors, actuation of microelectronic mechanical systems (MEMS), tissue engineering and screening tools.⁴⁷

When a biological fluid that contain proteins encounters a synthetic surface, proteins are primarily the first to interact with it by spontaneously adsorbing on the surface (chemical or foreign material sensing).⁴⁸ Adsorption of proteins on man-made surfaces during diagnosis and/or treatment of disease can be irreversible and if uncontrolled can result to dire consequences for example device failure and health risks to patients.⁴⁹ Scientific approaches to unlocking the mystery behind surface chemistry and protein

adsorption on synthetic surfaces is dependent on three factors. These factors include knowledge of structure and properties of subject proteins (for example conformation, type of functional groups present or polarity and stability), effective control and modification of surface properties of materials to mirror the relevant biochemistry of proteins, and availability of techniques (such as surface plasmon resonance spectroscopy and fluorescence microscopy) for monitoring in situ and real time protein adsorption on biomaterials.⁴⁹

Studies on proteins at molecular level is indisputably a complex endeavor especially in maintaining their natural bioactivity while investigating their properties. Protein patterning is regarded as the best strategy for studying interaction of surfaces of biomaterials with proteins. The patterning process relies on the ability to selectively adsorb proteins on appropriate sites on the material's surface and the ability of other sites of the surface to resist adsorption simultaneously. Proteins can reversibly or irreversibly adsorb on a surface through covalent bonds, electrostatic forces and bio-specific linkages.¹⁸ Covalent adsorption underpin the biomolecule on the surface causing non-specific adsorption and could reduce the activity of the protein.⁵⁰ Non-specific adsorption has been cited for reduced device signals and failure of devices.

Examples of protein patterning techniques include microcontact printing, conventional photolithography^{51, 52} and nanosphere lithography.¹⁸ Microcontact printing uses elastomeric material (stamp or mold) to fabricate patterns on self-assembled monolayers grown on a substrate and then immobilize proteins on the created patterns. In photolithography proteins adsorbed on a substrate are exposed to light of a given wavelength to generate desired patterns. It can also work by immobilizing proteins on

surfaces such as silicon that have been fabricated by UV light.⁵² Nanosphere lithography is the patterning technique used in this research for fabricating large scale protein patterns on self-assembled monolayers of alkytrichlorosilane (oxidized undecenyltrichlorosilane). Polystyrene nanospheres were used as mask. Several studies have fabricated proteins on mixed and/unmixed SAMs.^{53,54} Patterning based on nanosphere lithography is preferred because it doesn't require specialized equipment such as elastomers used in micro-contact printing and can create features to sub-100 nm as well as large-surface coverage as demonstrated by Cai et al when he used polystyrene nanospheres as masks. The nanospheres form a cohering mass on the surface of the SAMs thereby restricting deposition processes and chemical modification directly underneath them.⁵⁴

Deposition material used in this research is lysozyme from chicken egg white. Lysozyme is a small enzyme (its molecular mass is 14,307 Da) found in animal fluids such as tears, saliva, mucus and egg-white. It is commonly known for its anti-bacterial properties (lysozyme attack bacteria's (especially gram positive bacteria) cell walls by breaking the carbohydrate chains making up the walls). Because it is easily available and stable over a broad pH range (6.0-9.0), lysozyme is ideal for research involving protein structure and function. Lysozyme is composed of 129 amino acids cross-linked with four disulfide bonds.⁵⁵⁻⁵⁷ **Figure 4.1** shows 3-D structure of lysozyme.

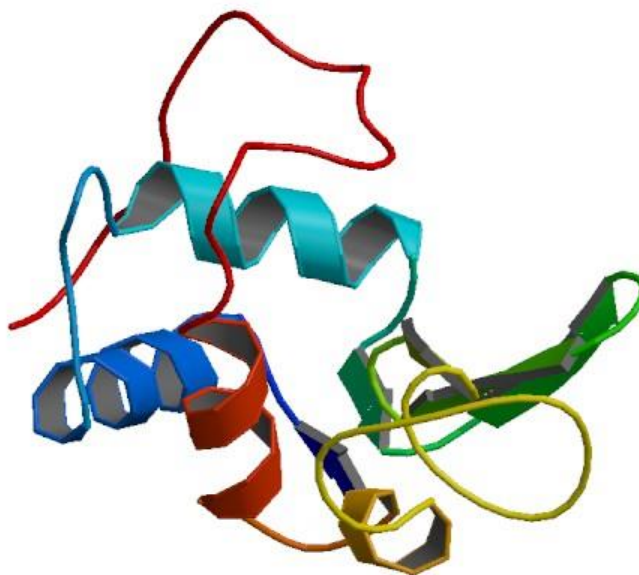


Figure 4.1. 3-D structure of lysozyme.⁵⁶

4.2 Experimental I: Nanofabrication of protein patterns on UTSox

4.2.1 Materials

Silicon (100) wafers (p-type virgin test grade) were purchased from university wafers. UTS was obtained from Gelest Inc., 11 Steel Rd. East, Morrisville, PA. while toluene (spectrophotometric grade 99+%) was from Acros Organics. UTSox was prepared in our lab as outlined in the previous chapter. Polystyrene nanospheres -900 nm- (solids 10.11%) and 500 nm silicon nanospheres (10 mg/ml) were purchased from Bangs Laboratories, Inc., and NanoComposix 4878 Ronson Ct, San Diego, CA 92111 respectively. Millipore water (18.2 M Ω .cm at 25 °C) was used in the entire preparation process. Hydrazine (anhydrous 98%) and 1-pyrenyldiazomethane (3 Mm), Lysozyme (5

μM in water), and fluorescein isothiocyanate (FITC) were bought from Sigma Aldrich Co. LLC. Nikon 80i fluorescence microscope was used for characterization.

4.2.2 Procedure I: Immobilization of Lysozyme

Before fabrication of lysozyme patterns, the protein was labelled with FITC (molecular weight 389 g/mol; see **Figure 4.2** for structure). The labelling was done at University of Kentucky. Protocol for tagging the protein with the dye involves drop-wise addition of 0.1 M FITC in dimethyl sulfoxide to 10 ml of 2 mg/ml lysozyme solution in sodium phosphate buffer containing 3% dimethyl sulfoxide. The reaction is conducted in ice water bath. After the reaction the mixture was stirred for 10 hours in the dark at 4°C. FITC is covalently linked to N-terminal amino group of lysozyme. Unbound FITC is removed through gel filtration chromatography.⁵⁷ The anchored dye fluoresce when excited by a fluorescent light hence characterization using a fluorescence microscope is made possible.

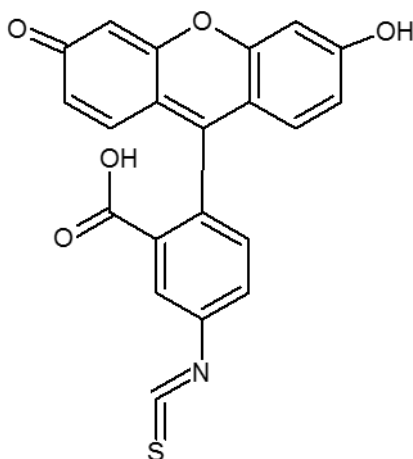


Figure 4.2. Structure of fluorescein isothiocyanate (FITC).

The procedure we used in fabrication of protein nano-features is quite similar to that used by Cai et al⁵⁴. Immobilization of lysozyme on UTSox was done by applying 1.5 μL of a solution of 0.9 μm polystyrene nanospheres on the surface. The sample was then covered to prevent dust contaminants from settling on the nanospheres and left overnight to dry slowly which would also ensure uniform spread of the nanospheres on the surface. In the next day, a few drops of FITC-lysozyme were applied on the nanospheres. FITC-lysozyme spreads on the nanospheres as well as in the interstitial spaces of the spheres. Lysozyme has an isoelectric point of 11.35⁵⁶ and would therefore electrostatically adsorb on the negatively charged carboxylic group of UTSox in the interstitial spaces of the nanospheres. **Figure 4.3** and **Figure 4.4** outline how the process was conducted.

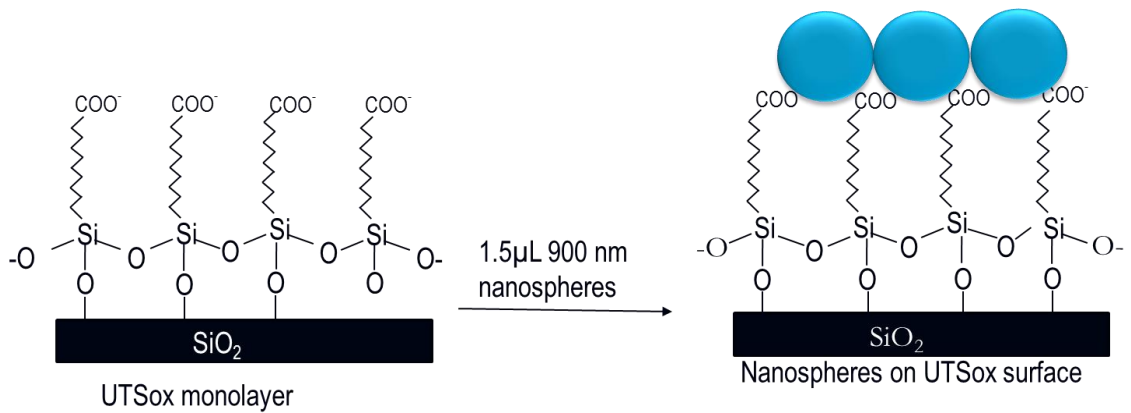
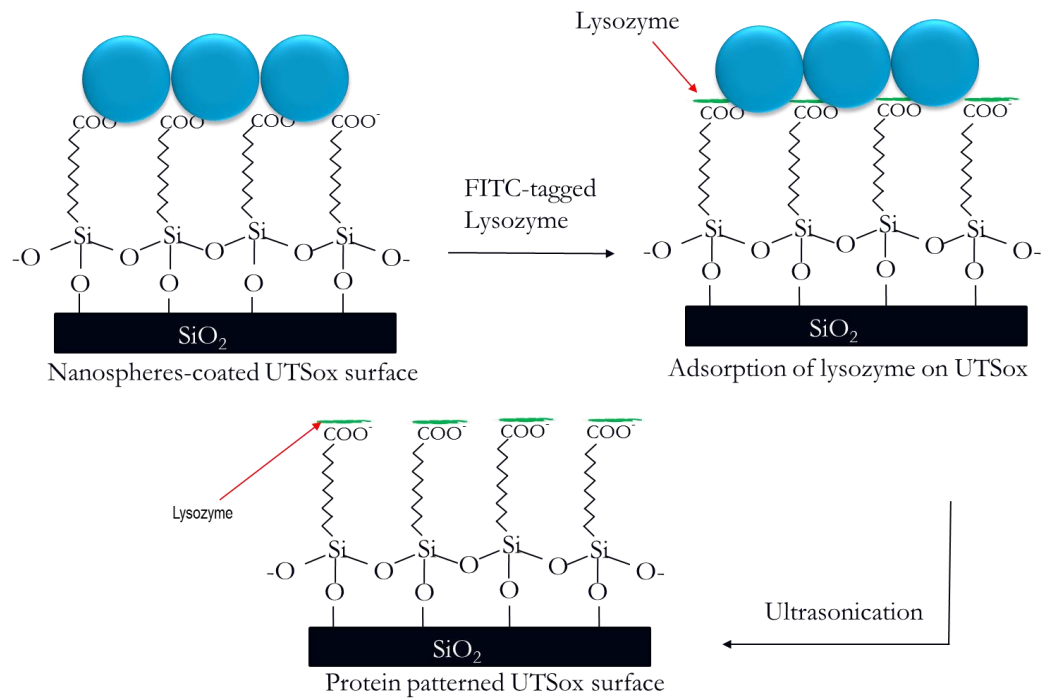


Figure 4.3. Illustration of coating of UTSox with polystyrene nanospheres



http://www.nature.com/scientificdata/2014/02/000001a
 Accessed 11/05/2014

Figure 4.4. Illustration of fabrication of lysozyme patterns on UTSox.

4.2.3 Characterization of protein patterns.

Characterization of FITC-tagged lysozyme was done using fluorescence microscope. Fluorescence images obtained are presented in **Figure 4.5**.

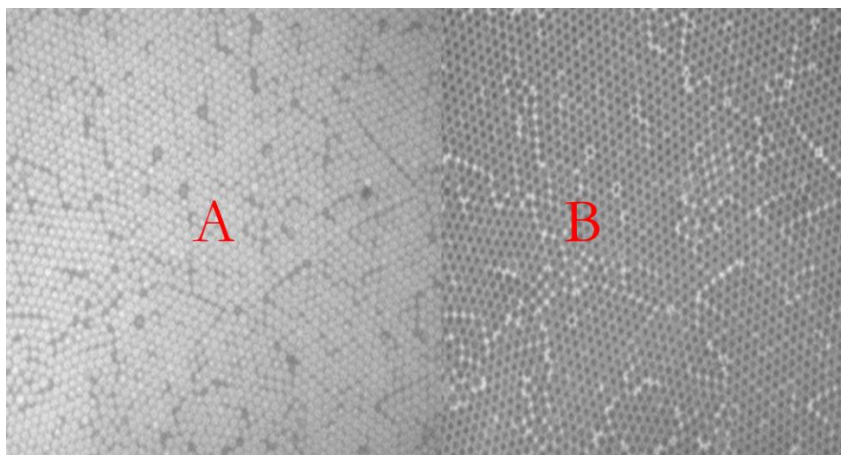


Figure 4.5. Fluorescence image of FITC-tagged lysozyme. Part A represents images taken against white light and B is taken against fluorescent light.

Image of FITC-tagged lysozyme taken against white light shows the nanospheres as bright spots (part A in the above figure) and interstitial area as dark. The nanospheres appear to have formed ordered aggregates on the surface. When taken against fluorescent light, the parts covered by the nanospheres is dark while interstitial areas appear bright, pointing out that lysozyme adsorbed on the spaces between the nanospheres.

Characterization was followed by removal of nanospheres through ultrasonication leaving behind patterns of holes (negative) and carboxylic-lysozyme. The activity of the immobilized lysozyme on $1 \times 1 \text{ cm}^2$ wafer samples was tested using fluorescence microscopy. To test the activity of lysozyme we propose the use of a commercially available lysozyme Assay Kit (E22013) from Invitrogen. Activity of lysozyme is 100 000 units/mg (one lysozyme activity unit is defined in this case as 0.001 absorbance drop in 450 nm per minute at pH 7 buffer at 25 °C, when measured by UV-Vis spectrometer using 1 cm optical path against *M. Luteus*).

Lysozyme Assay Kit (E22013) from Invitrogen detect lysozyme activity concentration as low as 30 U/ml. Our immobilized protein is projected to have covered at least 25% of the substrate's surface. Estimated lysozyme surface area is $5 \times 3 \text{ nm}^2$ corresponding to $\sim 40 \text{ ng}$ of the protein in $1 \times 1 \text{ cm}^2$ substrates. This translates to an activity of about 4 U/ml per sample. A drop of the substrate would be put into the sample and allowed to react for 10 minutes. The equivalent lysozyme concentration in the drop would be 800 U/ml which is above the lowest detectable amount. After 10 minutes of reaction, the solution would be transferred to micro-cuvette and measured by spectrofluorometer. The measured values will be compared with pre-calibrated standard lysozyme activity-fluorescence signal curve to figure out the actual lysozyme activity.

4.3 Experimental II: Preparation of multilayers of self-assembled monolayers.

4.3.1 Materials

The materials used in this section are the same as those described under section 4.2.1.

4.3.2 Procedure II: Preparation of OTS Layer on UTSox

In this section we combine solution and chemical vapor deposition (CVD) methods to grow octadecyltrichlorosilane monolayers on oxidized undecenyltrichlorosilane (see **Figure 4.6** for illustration). As has been noted earlier presence of trace amounts of water (it is difficult to completely get rid of water in solution phase) in solution-based reaction media would interfere with film uniformity. The method is also marred by accumulation

of multilayers or 3-D molecular aggregates which are difficult to remove by ultrasonication once formed. Chemical vapor deposition regime minimizes water condensation on the substrate and consequently produces more uniform films. It also reduces formation of multilayers or 3-D molecular aggregates.⁵⁸

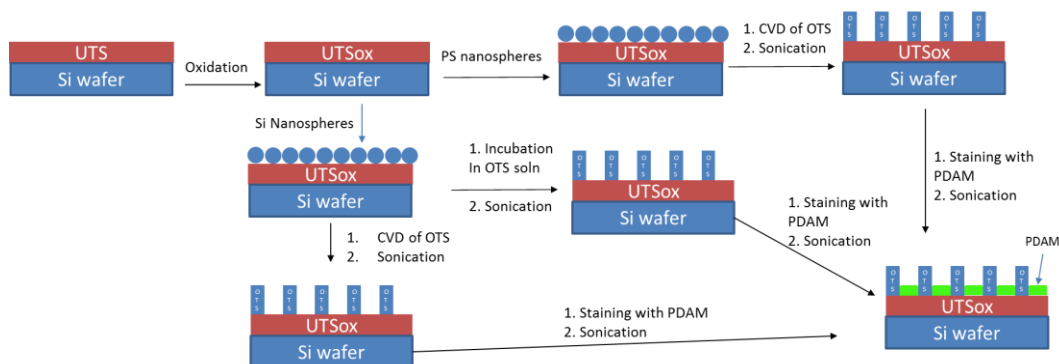


Figure 4.6. Schematic representation for preparation of multi-layers of SAMs.

Procedure for preparation of Undecenyltrichlorosilane SAMs on $1 \times 1 \text{ cm}^2$ Si(100) wafer and its oxidation to UTSox was described in chapter 3. We want to grow a layer of octadecyltrichlorosilane (OTS) on top of UTSox surface through two approaches; solution and vapor deposition. For chemical vapor deposition approach, polystyrene nanospheres (900 nm) were uniformly spread over UTSox samples. Next, polystyrene coated samples were transferred into a small vial. The vial was then inserted into a relatively bigger vial containing 1 ml of pure OTS. The small vial was left open but the bigger one was tightly closed. We placed the sample into an oven and allowed to stand overnight (12 hours) at 100°C and 21.325 kPa. The high temperature is intended to increase vaporization of OTS. This constituted our chemical vapor deposition system. Octadecyltrichlorosilane molecules

would adsorb to the carboxylic acid groups of UTSox presented on the interstitial spaces of the nanospheres. Images of the samples were taken against white light using a fluorescence microscope. Because polystyrene nanosphere are soluble in toluene, solution phase approach for growing OTS on UTSox patterned with polystyrene nanospheres is not suitable here.

In our second approach, UTSox samples were coated with 500 nm silicon nanospheres and immersed in 5 mM OTS in toluene and incubated for 12 hours at room temperature condition. Silicon nanospheres do not dissolve in toluene thus solution phase deposition of OTS on silicon patterned substrates would not interfere with the nanospheres. CVD was also used to develop OTS on silicon patterned UTSox substrates. The procedure and conditions for CVD of OTS on silicon-patterned UTSox are as stated in the case of polystyrene coated samples.

After preparation of OTS in all the three cases, the nanospheres were removed by ultra-sonication. Ultrasonication was done for 30 seconds. Removal of nanospheres exposes the UTSox layer that was directly beneath the nanosphere. At this point, we have obtained mixed surface properties because $-CH_3$ (from UTSox-OTS) and $-COOH$ (from UTSox) terminal groups are exposed. To confirm the formation of UTSox-OTS we anchored a fluorescent dye (PDAM) on the surfaces of our samples. This was done by immersing the samples into 3 mM of PDAM in methanol and incubated for 12 hours. PDAM reacts with the carboxylic acid group of the UTSox as shown earlier in chapter 3. After the incubation period samples were remove from the PDAM solution. This is followed by ultra-sonication to remove non-specific adsorption of PDAM molecules.

4.3.3 Characterization of OTS-UTSox multi-layers

Uniformity of polystyrene and silicon nanospheres on UTSox samples was gauged using fluorescence microscope. The images obtained are presented in **Figure 4.7**. Polystyrene nanospheres appeared bright while silicon nanospheres appeared dark. We did not know why the silicon nanospheres showed a negative image yet the spheres are supposed to produce a positive image as reported by the manufacturer.

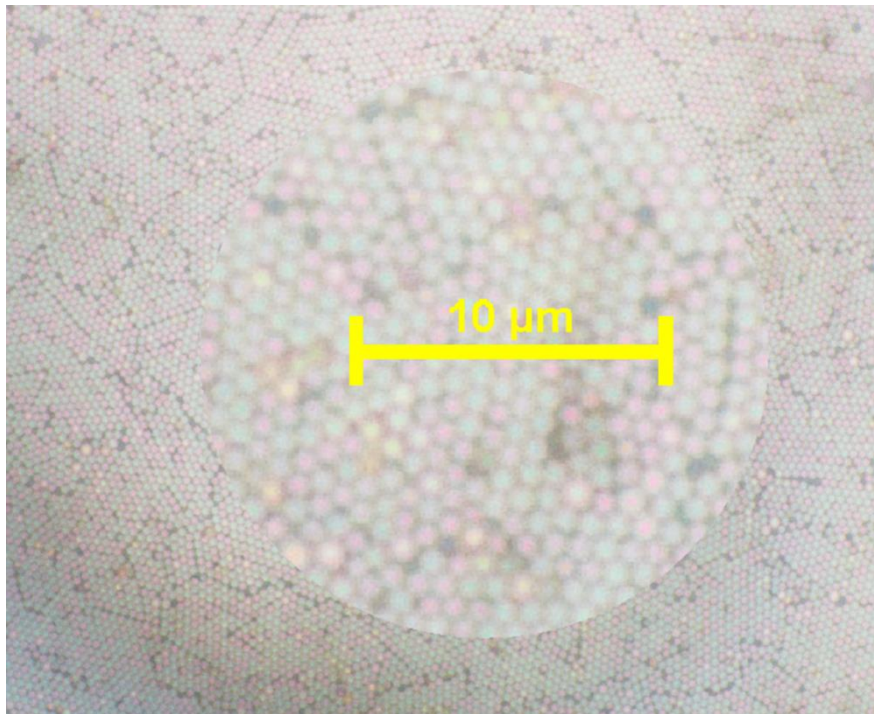


Figure 4.7. Polystyrene nanospheres on UTSox.

The nanospheres formed closely packed arrays on the surface. A closer look at the scale shows approximately eleven nanospheres are within the shown scale bar. The image also shows point and line defects (linear uncovered parts in the diagram) within the

nanoparticles. The defects would decrease uniformity of patterns generated. However our patterns are good enough for protein patterning.

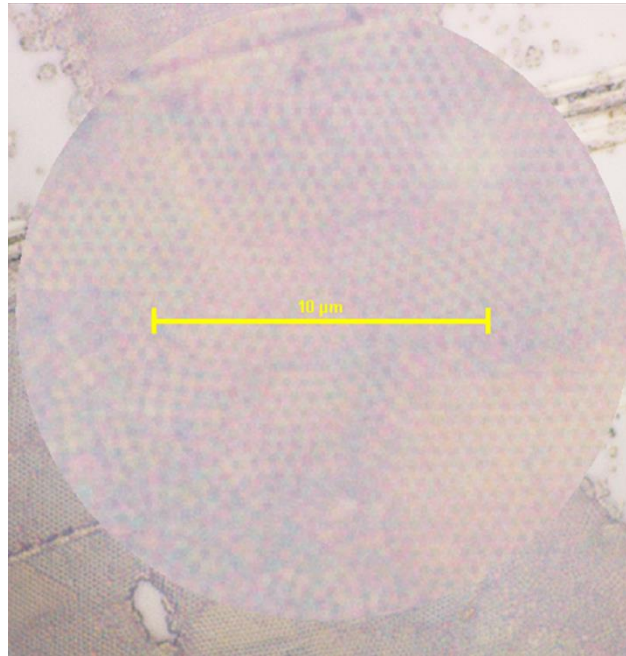


Figure 4.8. Image of silicon nanospheres on UTSox surface.

Unlike polystyrene nanospheres that appeared to have covered the whole silicon wafer, our silicon nanospheres image shows the nanoparticles did not extensively cover the whole sample's surface. This can partly be attributed to the smaller size of silicon nanoparticles compared to polystyrene nanospheres. The image presented in **Figure 4.8** is obtained by zooming in a region occupied by silicon nanospheres. Nonetheless the nanospheres have produced compact arrays on the sample's regions covered.

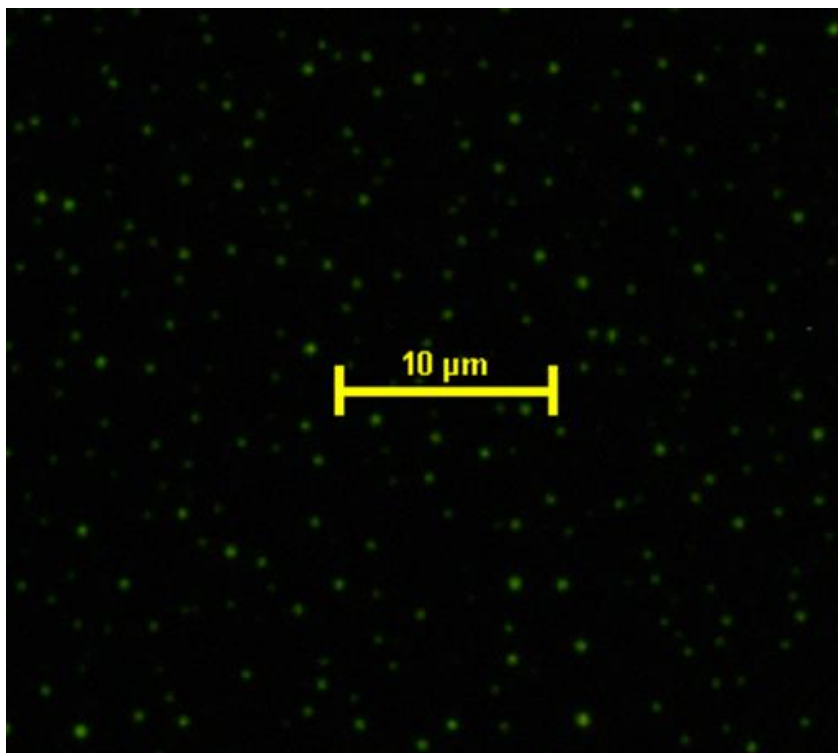


Figure 4.9. Fluorescence images of polystyrene patterned OTS-UTSox. The green dots indicates parts of the sample which was not occupied by OTS. The center part of the image has been magnified.

The OTS molecules would adsorb on the hydroxyl group of UTSox between the nanospheres. After removal of the nanospheres, the sample was stained with PDAM then characterized using a fluorescence microscope to obtain the image shown in **Figure 4.9**. The green dots represent regions occupied by the fluorophore (PDAM) which are the regions occupied by UTSox. These regions are the ones which were earlier occupied by nanospheres. The purpose of the nanospheres was to prevent extensive bonding of OTS with UTSox directly beneath the spheres. The scale bar represent a distance occupied by eleven nanospheres as reported earlier. The developed OTS-UTSox molecular assemblies

do not fluoresce. These assemblies are therefore present on the dark (black) parts of the diagram.

Figure 4.10 has been obtained the same way as **Figure 4.9**, but we used silicon nanospheres in this case; the two figures are actually the same in principle. The inset shows a relatively larger number of green dots per unit area compared to polystyrene patterned surface due to the smaller size of silicon's spheres. Approximately 20 silicon spheres can fit the shown scale bar distance.

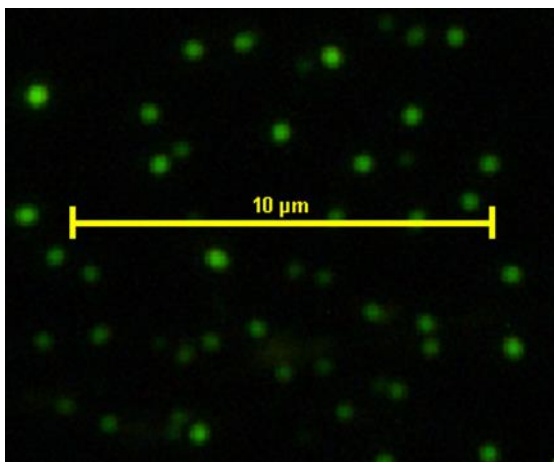


Figure 4.10. Fluorescence Image of silicon patterned UTSox sample. A circular zoomed inset is at the center of the image (enlarged green signals).

The images confirm formation of OTS layer on UTSox, otherwise the PDAM fluorescence signs would have covered the whole substrate's surface.

4.4 Conclusion

Protein patterns were obtained by combining silane chemistry (as in development of self-assembled molecular assemblies) and nanosphere lithography. Formation of nanometer patterns was confirmed using fluorescence microscopy. By use of smaller nanospheres (say 200 nm diameter or smaller) further features' size reduction can be achieved. Lysozyme protein has a net positive charge which enables it to electrostatically adsorb to the negatively charged carboxylic acid group of UTSox. Lysozyme can also be patterned on the multi-layers of UTSox and OTS-UTSox self-assembled monolayers. The methyl terminal group of OTS-UTSox would repel polar proteins. The repulsion would be capitalized by the carboxylic acid group of UTSox to bond with the SAMs thus producing uniform patterns. A polar macromolecule can also be patterned on the same surface whereby it would interact with the methyl group (terminal group) of OTS-UTSox bilayer.

Usefulness of nanosphere lithography here is not only linked to its simplicity and high throughput but also its immense application in diverse disciplines and industries. It is the success of effective anchoring of protein on surfaces of man-made devices that powers the health sector in development of synthetic tissue organs, biosensors, diagnostic arrays and drug delivery. Our patterned silicon wafer can be used to probe surface containing lysozyme antibodies.⁴⁸ Further investigation of more complex proteins other than lysozyme using nanosphere lithography could pave way for a better understanding of interaction of biomolecules with materials.

CHAPTER 5

CONCLUSION AND FUTURE DIRECTIONS

5.1 Conclusions

The extend of nanosphere lithography's research has undergone a dramatic increase for the last two decades following Richard van Duyne et al's demonstration of the generality of the process on materials. Driven by its relatively low costs, the process is perceived as the best alternative for fabrication of nano-meter level features. We have utilized the process in fabrication of packed lysozyme patterns on self-assembled monolayers terminated with carboxylic functional group, that were developed using 'bottom-up' approach. Lysozyme was attached to the SAM through Coulombic's force (physical attachment).

Vinyl terminated alkyltricholasilane monolayers were grown through solution phase and further modified to produce the carboxylic functional group. Monolayers of this type have a great advantage in further modification of surface properties of self-assembled monolayers. Other functional groups that can be developed through modification of the vinyl group include halides (Br^- , Cl^-), alcohol ($-\text{OH}$), alkyl ($-\text{CH}_3$) and amines ($-\text{NH}_2$). The modification means various proteins features can be mimicked on such monolayers. For instance, hydrophobic and hydrophilic neutral proteins can be modelled on methyl ($-\text{CH}_3$) and hydroxyl ($-\text{OH}$) terminated surfaces, while carboxylic ($-\text{COOH}$) and amine ($-\text{NH}_2$)

terminated surfaces are good for positively and negatively charged biomolecules respectively. The choice of the terminal group to be used depends on the properties of biomolecules under research.⁵⁹

The success of protein patterning based on nanosphere lithography is also influenced by availability of characterization techniques. While Fourier-Transform can be used to identify surface functional groups, atomic force microscope ameliorates the understanding of the process by revealing how small the nanostructures or microstructures are. Another useful tool that can provide real time tracking of patterning is the fluorescence microscope. As noted in earlier chapters, our protein and SAM-COOH were dyed with FITC and PDAM respectively because none of them could produce a fluorescence signal of its own. A combination of these three techniques in our research enabled us to confirm the production of nano-features of both self-assembled monolayers and proteins.

5.2 Challenges of the Research

Though nanosphere lithography is flexible and relatively easy to handle, there were seldom avertible challenges that negatively affected our results. At the forefront is pattern defects which result from incoherent arrangement of nanospheres on the surfaces. Slip dislocation of nanospheres causes line defects (shown in **Figure 5.1**) while point defects arise from vacancies (unoccupied parts within the arrays of the spheres). Size and spacing of mask holes go hand in hand hence cannot be independently controlled.⁶¹⁻⁶³

The defects arising from nanosphere lithography can be explained in terms of the forces responsible for the spread of the nanospheres on surfaces. Van der Waals may cause

aggregation of the nanoparticles within the suspension or on the substrate's surface leaving it with sporadic lumps of mono- or multi-layers of nanospheres (3D particle aggregates). Ordering of the spheres as the solvent evaporates can be interfered by rate of evaporation. In this case capillary action (resulting from surface tension of solvent and nanospheres) may be hastened by high evaporation rate of solvent which in turn hampers development of regular patterns. In other words capillary forces compacts particles into small 2D aggregates and voids, an intense process that can even cause particle deformation.⁶⁴The defects makes generation of large-scale patterns and its reproducibility a really challenging task.

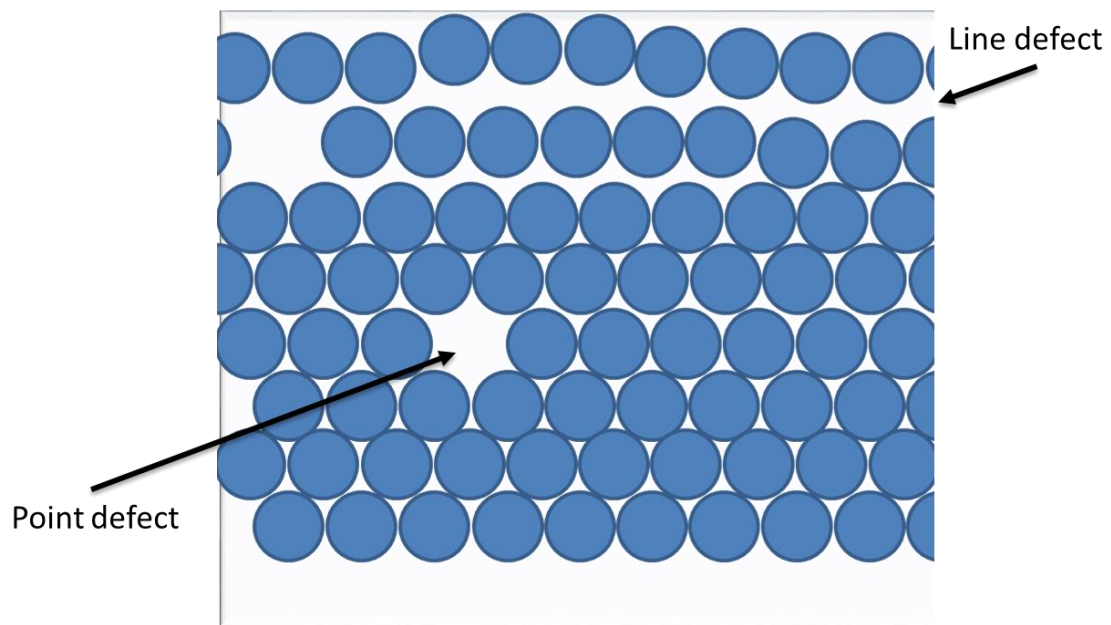


Figure 5.1. Illustration of point and line defects in nanospheres patterns.

Fluorescence image of UTSox-PDAM displayed an irregular pattern over large area. By zooming the image at certain regions we were able to obtain more uniform patterns whose regularity falls short of large-scale. Nonetheless our images qualitatively demonstrate the potential of nanosphere lithography in fabricating nanofeatures. Additionally, earlier patterns obtained from patterning of lysozyme were more regular over large scale.

Pattern defects is a challenge faced by almost every research group dealing with nanosphere lithography. Though hardly avoided, nanotechnologists have schemed state of the art ways of minimizing the defects more so in modulating evaporation rates of the solvent. Atanassov et al used a specialized model to spread nanospheres over the substrate's surface. The set-up is designed such that the substrate forms an angle of 23° with a movable plate. A suspension of nanoparticles was placed at the junction and the plate is moved along the substrate to spread the nanoparticles as the solvent evaporates. Though time-consuming the method minimized formation of irregular features.^{65,66}

5.3 Future Directions

Having demonstrated creation of lysozyme patterns on UTSox, we are set to test the bioactivity of the protein using lysozyme Assay Kit (E22013) from Invitrogen. We will also investigate duration over which bioactivity of the patterned protein could be retained under given conditions. Ability to maintain bioactivity of immobilized proteins is pivotal as far as development of biosensors is concerned. Lysozyme immobilized on a substrate can function as a biosensor for lysozyme antibodies.

5.4 Concluding Remarks

Nanosphere lithography has been demonstrated as a good form of nanotechnology for studying molecular properties of materials. Its low cost and ability to produce sub-100 nm features places it above other conventional methods like photolithography. Relentless efforts to minimize its demerits is key to successful development of large-scale patterns and in turn expanding its application. With myriad research groups working on improving the technique; motivated by love for ever-shrinking device sizes and improved sensitivity, nanosphere lithography is in no doubt destined to improve the quality of human-life.

REFERENCES

1. Duyne, R. P. V.; Hulteen, J. C. Nanosphere Lithography: A Material General Fabrication Process for Periodic Particle Array Surfaces. American Vacuum Society, **1995**, 13, 3, 1553-1558.
2. Duval, M. C.; Duyne, R. P. V.; Hulteen, J. C.; Jensen, T. R.; Smith, M.T.; Treichel, D. A. Nanosphere Lithography: Size-Tunable Silver Nanoparticle and Surface Cluster Arrays. *J. Phys. Chem. B* **1999**, 103, 3854-3863.
3. Duyne, R. P. V.; Haynes, C. L. Nanosphere Lithography: A Versatile Nanofabrication Tool for Studies of Size-Dependent Nanoparticles Optics. *J. Phys. Chem. B* **2001**, 105, 5599-5611.
4. Bradford, R. W.; Duncan, J. P. Simplified Strategic Planning: A No-Nonsense Guide for Busy People Who Want Results Fast! Chandler House Press, Worcester, MA, 2000, pg 127.
5. Feynman, R. P. There's Plenty of Room at the Bottom. *Caltech Engineering and Science*, **1960**, 23, 5, 22-26.
6. Cloots, R.; Colson, P.; Henrist, C. Nanosphere Lithography: A powerful Method for the Controlled Manufacturing of Nanomaterials. *Journal of Nanomaterials*, **2013**, 2013, 1-19.
7. University of Washington, Electrical Engineering. <https://www.ee.washington.edu/research/microtech/cam/PROCESSES/PDF%20FILES/Photolithography.pdf>. (Accessed 3/30/2015).
8. Barron, A. R. Optical Issues in Photolithography. http://cnx.org/contents/0661ebbe-52fb-48b1-a96a-0878fa6270ed@4/Optical_Issues_in_Photolithog#id1164120248912. (Accessed 3/30/2015).
9. Mack, C. Fundamental Principles of Optical Lithography: The Science of Microfabrication. John Wiley & Sons Ltd., The Atrium, Southern Gate, Chichester, West Sussex, England; 2007, pp 1-4.
10. Harriott, L. R. Limits of Lithography. *Proceedings of the IEEE*, **2001**, 89, 3, 366-374.
11. Chen, C. D.; Chen, K.; Ma, K. J.; Tseng, A. A. Electron Beam Lithography in Nanoscale Fabrication: Recent Development. *IEEE Transactions On Electronics Packaging Manufacturing*; **2003**, 26, 2, 141-149.
12. Pimpin, A.; Srituravanich, W. Review on Micro- and Nanolithography Techniques and Their Applications. *Engineering Journal*; **2012**, 16, 1.
13. Deckman, H. W.; Dunsmuir, J. H. Natural Lithography. *Applied Physics Letters*; **1982**, 41, 4, 377-379.
14. An, H. M.; Kim, T. G.; Sim, J. I.; Yang, J. W. Fabrication of Nanometer-scale Pillar Structures by Using Nanosphere Lithography. *Journal of the Korean Physical Society*, 2011, 58, 4, 994-997.
15. Duyne, R. P.V; Hicks, E. M.; Whitney, A. V.; Zhang, X.; Zhao, J. Advances in contemporary Nanosphere Lithographic Techniques. *Journal of Nanoscience and Nanotechnology*, **2006**, 6, 1-15.

16. Eilers, J. E.; Sellers, H. Shnidman, Y.; Ulman, A. Structure and Binding Alkanethiolates on Gold and Silver Surfaces: Implication for Self-Assembled Monolayers. *J. Am. Chem. Soc.* 1993, 115, 9389-9401.
17. Estroff, L. A.; Kriebel, J. K.; Love, J. C.; Nuzzo, R. G.; Whitesides, G. M. Self-Assembled Monolayers of Thiolates on Metals as a Form of Nanotechnology. *Chem. Rev.* **2005**, 105, 1103–1169.
18. Gao, P. Fabrication and Characterization of Mesoscale Protein Patterns Using Atomic Force Microscopy (AFM). University of Kentucky Doctoral Dissertation, **2011**, 1-148.
19. Allara, D. L.; Nuzzo, R. G. Spontaneously Organized Molecular Assemblies. 1. Formation, Dynamics, and Physical Properties of n-Alkanoic Acids Adsorbed from Solution on an Oxidized Aluminum surface. *Langmuir*, 1985, 1, 45-52.
20. Ulman, A. Formation and Structure of Self-Assembled Monolayers. *Chem. Rev.* **1996**, 96, 1533–1554.
21. Ghiran, I. C. Introduction to Fluorescence Microscopy. *Light Microscopy: Methods and protocols*, Atlas Systems, Inc. 2011, pp 93-136.
22. Conchello, J. A.; Lichtman, J. W. Fluorescence Microscopy. *Nature methods*, 2005, 2, 910-919.
23. Hell, W. S. Toward Fluorescence Nanoscopy. *Nature Biology*, 2003, 21, 1347-1355.
24. Masters, B. R. The Development of Fluorescence Microscopy. *Encyclopedia of Life Sciences*, John Wiley & Sons, 2010, 1-9.
25. Basic Photophysics. <http://www.photobiology.info/Visser-Rolinski.html>. (Accessed 02/22/2015).
26. Spring, K. R. Fluorescence Microscopy. *Encyclopedia of Optical Engineering*, Marcel Dekker Inc. 2003; pp 548-555.
27. Crouch, S. R.; Holler, F. J.; Skoog, D. A. Principles of Instrumental Analysis, 6th ed.; Thomson Brooks/Cole: Belmont, Canada, 2007; pp 430-478.
28. Klein, D. Organic Chemistry. John Wiley & Sons, Inc., 2012; pp. 672-694.
29. Coates, J. Interpretation of Infrared Spectra, a Practical Approach. *Encyclopedia of Analytical Chemistry*, R.A Meyers (Ed.): John Wiley & Sons Inc., 2000; pp. 10815-10837.
30. Kroschwitz, J. I. I. Infrared Spectroscopy. *Kirk-Othmer encyclopedia of chemical technology*: John Wiley & Sons, Inc., 2005; 14, 1-20.
31. Harris, D. C. Quantitative Chemical Analysis, 8th ed.; W. H. Freeman and Company, New York, 2010; pp 396-397.
32. ThermoNicolet. <http://mmrc.caltech.edu/FTIR/FTIRintro.pdf>. (Accessed 02/25/2015).
33. Bottomley, L. A.; Coury, J. E.; First P. N. Scanning Probe Microscopy. *Anal. Chem.* 1986; 68, 185-230.
34. Binning, G.; Gerber C.; Quate, C. F. Atomic Force Microscope. *Physical Letters Reviews*, 1986; 56, 930-933.
35. Blanchard, C. R. Atomic Force Microscopy. *The Chemical Educator*: Springer-Verlag, New York Inc., 1996; 1, 1-8.
36. Alvarez, L.; Squeiros, J. M. Scanning Probe Microscopy. *Formatex*, 2010; 1302-1309.

37. Hansman, P.; Rugar, D. Atomic Force Microscopy. American Institute of Physics: Physics Today, 1990; 23-30.
38. Benatar, C.; Howland R. A Practical Guide to Scanning Probe Microscopy. ThermoMicroscopes, 2000; 5-13.
39. Meyer, E. Atomic Force Microscopy. Progress in Surface Science, 1992; 41, 3-49
40. Chapman, R. G.; Ostuni, E.; Whitesides, G. M.; Yan, L. Preparation of Mixed Self-Assembled Monolayers (SAMs) That Resist Adsorption of Proteins Using the Reaction of Amines with a SAM That Presents Interchain Carboxylic Anhydride Groups. Langmuir 2000, 16, 6927-6936.
41. Tao, Y. -T.; Wasserman, S. R.; Whitesides, G. M. Structure and Reactivity of Alkylsiloxane Monolayers Formed by Reaction of Alkyltrichlorosilanes on Silicon Substrates. Langmuir 1989, 5, 1074-1087.
42. Brugger, J.; Huskens, J.; Kim, B. J.; Liebau, M.; Reinhoudt, D. N. A Self-assembled Monolayer-assisted surface microfabrication and release technique. Microelectronic Engineering, 2001, 57-58, 755-760
43. Dosch, H.; Honkimaki, V.; Mezger, M.; Okasinski, J.; Palms, J.; Ralston, J.; Reichert, H.; Schoder, H.; Schoder, S. High-resolution in situ x-ray study of the hydrophobic gap at the water-octadecyl-trichlorosilane interface. PNAS, The National Academy of Science, 2006; 103, 49, 18401-18404.
44. Boo, J. H.; Kim, S.; Lee, J.; Sohn, H. Significantly improved stability of n-octadecyltrichlorosilane self-assembled monolayer by plasma pretreatment on mica. Thin Solid Films, 2008, 516 940-947.
45. http://faculty.southseattle.edu/sendsley/Organic_Lecture_files/Chapter12_McMurry_Part2.pdf. (Accessed 3/15/2015).
46. Hallen, H. D.; Hallen, M. A. Synthesis of Carboxylic Acid Monolayers by Ozonolysis of 10-undecenyltrichlorosilane SAMs. J. Phys. Chem. C; 2008, 112, 2086-2U ODFJ5090.
47. Cheng, L-J.; Guo, L. J.; Hoff, J. D.; Hunt, A. J.; Meyhofer E. Nanoscale Protein Patterning by Imprint Lithography. Nano Lett., 2004, 4, 5, 853-857.
48. Alexander, M.; Kingshott, P.; Ogaki, R. Chemical Patterning in Biointerface Science. Materials Today, 2010, 13, 4, 22-35.
49. Mrksich, M.; Whitesides, G. M. Using Self-Assembled Monolayers to Understand the Interactions of Man-Made Surfaces with Proteins and Cells. Annu. Rev. Biophys. Biomol. Struct. 1996, 2555-78.
50. Davies, M. C.; Hartsborne, M.; Heaton, R. J.; Patel, N.; Roberts, C. J.; Tendler, S. J. B.; Williams, P. M. Immobilization of Protein Molecules onto Homogeneous and Mixed Carboxylate-Terminated Self-Assembled Monolayers. Langmuir 1997, 13, 6485-6490
51. Veiseh, M.; Zareie, M. H.; Zhang, M. Highly Selective Protein Patterning on Gold-Silicon Substrates for Biosensor Applications. Langmuir 2002, 18, 6671-6678.
52. Ingber, D. E.; Kane, R. S.; Ostuni, E.; Takayama, S.; Whitesides, G. M. Patterning of proteins and cells using Soft Lithography. Biomaterials 20, 1999, 2363-2376.
53. Arima, Y.; Iwata, H. Effects of Surface Functional Groups on Protein Adsorption and Subsequent Cell Adhesion Using Self-Assembled Monolayers. Journal of Material Chemistry, 2007, 17, 4079-4087.

54. Cai, Y.; Ocko, B. M. Large-Scale Fabrication of Protein Nanoarrays Based on Nanosphere Lithography. *Langmuir* 2005, 21, 9274-9279.
55. David Goodsell & RCSB Protein Data Bank. <http://www.rcsb.org/pdb/101/motm.do?momID=9>. (Accessed 2nd April, 2015).
56. Sigma-Aldrich. <https://www.sigmaaldrich.com/content/dam/sigmaaldrich/docs/Sigma/Datasheet/7/17651dat.pdf> (Accessed 2nd April, 2015).
57. Murase, T.; Nishimoto, E.; Takahashi, D.; Yamashita, S. Protein-Protein Interaction on Lysozyme Crystallization Revealed by Rotational Diffusion Analysis. *Biophys J.*, 2008, 94, 11, 4484-4492.
58. Dong, J.; Mao, G.; Ng K. Y. S.; Wang, A. Self-Assembly of Octadecyltrichlorosilane Monolayers on Silicon-Based Substrates by Chemical Vapor Deposition. *Thin Solid Films*, 2006, 515, 2116-2122.
59. Chen, S.; Jiang, S.; Li, L.; Wang, H. Improved Method for the Preparation of Carboxylic Acid and Amine Terminated Self-Assembled Monolayers of Alkanethiolates. *Langmuir, ACS*, 2005, 21, 7, 2633-2636.
60. Duyne, R. P. V.; Myers, B. D.; Whitney, A. V. Sub-100 nm Triangular Nanopores Fabricated with the Reactive Ion Etching Variant of Nanosphere Lithography and Angle-Resolved Nanosphere Lithography. *Nano Letters*, 2004, 4, 8, 1507-1511.
61. Blaaderen, A. V.; Dillen, T. V.; Fific, D.; Penninkhof, J. Polman, A.; Vossen, D. L. J. Combined Optical Tweezers/Ion Beam Technique to Tune Colloidal Masks for Nanolithography. *Nano Letters*, 2005, 5, 6, 1175-1179.
62. Chen, A.; Chua, J. S.; Yan, Q.; Zhao, X. S. Nanosphere Lithography from Template-Directed Colloidal Sphere Assemblies. *J. Nanosci. Nanotechnol.* 2006, 6, 1815-1818.
63. Department of Materials Science and Engineering, Northwestern University, http://community.nsee.us/courses/3760_nanomaterials_sp04/nanoscale_optical_properties.pdf. (Accessed 03/23/2015).
64. Burkhardt, C.; Fuchsberger, K.; Nisch, W.; Stelzle, M. Micro- and Nanopatterning of Surface Employing Self Assembly of Nanoparticles and Its Application in Biotechnology and Biomedical Engineering, Lithography, Michael Wang (Ed.); InTech [Online], Germany, 2010; pp 631-644.
65. Atanassov, P.; Burckel, D. B.; Fan, H.; Yuan, Z. Convective Self-Assembly to Deposit Supported Ultra-Thin Mesoporous Silica Films. *Journal of Materials Chemistry*, 2006, 16, 4637-4641.
66. Prevo, B. G.; Velev, O. D. Controlled, Rapid Deposition of Structured Coatings from Micro- and Nanoparticle Suspensions. *Langmuir* 2004, 20, 2099-2107.